Science of Remote Sensing 11 (2025) 100219

Contents lists available at ScienceDirect

Science of Remote Sensing

journal homepage: www.sciencedirect.com/journal/science-of-remote-sensing

Full length article

Vegetation browning as an indicator of drought impact and ecosystem resilience

Ignacio Fuentes [a,b,*], Javier Lopatin [c,d,e], Mauricio Galleguillos [c,d,e], James McPhee [f,g]

[a] Facultad de Medicina Veterinaria y Agronomía, Universidad de Las Américas, Sede Providencia, Manuel Montt 948, Santiago, Chile
[b] Núcleo de Investigación en Sustentabilidad Agroambiental (NISUA), Universidad de las Américas, Santiago, Chile
[c] Facultad de Ingeniería y Ciencias, Universidad Adolfo Ibáñez, Santiago, Chile
[d] Fundación Data Observatory, Santiago, Chile
[e] Center for Climate and Resilience Research (CR2), Santiago, Chile
[f] Department of Civil Engineering, Faculty of Physical and Mathematical Sciences, University of Chile, Santiago, Chile
[g] Advanced Mining Technology Center, Faculty of Physical and Mathematical Sciences, University of Chile, Santiago, Chile

ARTICLE INFO

Keywords:
Vegetation browning
Remote sensing
Drought propagation
Change detection
Resilience

ABSTRACT

Climate change influences climate variability, increasing the frequency and severity of droughts. These events may trigger vegetation browning, a key indicator of drought propagation and shifts in resilience. While long-term trends often measure browning, rapid vegetation declines require alternative approaches. This study examines drought-induced vegetation browning, resilience, and propagation in central Chile using Moderate Resolution Imaging Spectroradiometer (MODIS) time series of normalised difference vegetation index (NDVI), leaf area index (LAI), and gross primary productivity (GPP). The Continuous Change Detection and Classification (CCDC) algorithm identified negative vegetation changes, filtering out non-browning events to reduce uncertainties. Spatial variations in browning were analysed across latitudinal gradients, topographies, and vegetation types, while shifts in temporal autocorrelation served as a proxy for resilience. Results indicated declines in NDVI across 19% of the study area, GPP in 12%, and LAI in 8%. NDVI responded to drought within six months, with productivity losses lagging by 8.7 months. Recovery was slow, averaging 3.6 years, and only 20%–25% of the affected areas recovered. Variations in browning timing and magnitude were driven by topography, vegetation, and latitude. A decline in vegetation resilience highlights the need for strategies to enhance adaptability to climate change.

1. Introduction

Vegetation in various regions is typically exposed to distinct stressors, which can result in degradation (Kofinas, 2009; Liu et al., 2013; Forzieri et al., 2022). While logging and deforestation represent direct anthropogenic pressures on vegetation, other prevalent causes of degradation include droughts and fires, both of which are influenced by natural processes and human activity (Carrión et al., 2010; Kumar et al., 2022). Droughts, that may be intensified by climate change, reduce water availability, leading to physiological stress in plants and ecosystem instability (Vicente-Serrano et al., 2020; Seleiman et al., 2021), while fires, natural or human-induced, can destroy vast vegetation areas, particularly during prolonged droughts or heatwaves, which may be worsened by global warming (Pausas and Keeley, 2021). Though interannual climate variability occurs naturally, leading to dry and wet meteorologic conditions, climate change has been implicated as an additional factor influencing climate variability (Thornton et al., 2014), and it may contribute to some drivers of vegetation deterioration (Vicente-Serrano et al., 2015; Vilanova et al., 2021).

Meteorological water deficits can propagate through various subsystems of the water cycle (Wang et al., 2016; Fuentes et al., 2022; Van Loon et al., 2024). Vegetation is affected by these deficits as they spread through terrestrial systems, impacting plant health and vigour (Zhang et al., 2022; Vicente-Serrano et al., 2013). This can result in decreased vegetation vitality or even mortality, which may be detectable through satellite-based reflectance analysis when these changes are significant (Xie et al., 2008). Consequently, water deficits can trigger vegetation browning, often implying changes in vegetation colour from green to brown (Pan et al., 2018; Cortés et al., 2021), which may indicate a change in vegetation dynamics and may also refer to negative trends in remotely sensed vegetation indices over time (Miranda et al., 2020; Liu et al., 2023a). However, browning can also indicate short-term declines in vegetation due to specific disturbances, often depicted

* Corresponding author at: Facultad de Medicina Veterinaria y Agronomía, Universidad de Las Américas, Sede Providencia, Manuel Montt 948, Santiago, Chile.
E-mail address: ifuentes@udla.cl (I. Fuentes).

https://doi.org/10.1016/j.srs.2025.100219
Received 10 December 2024; Received in revised form 19 February 2025; Accepted 14 March 2025
Available online 24 March 2025

in vegetation reflectance patterns (De Jong et al., 2012). Disturbances such as droughts can lead to vegetation stress and wilting, which can be monitored by assessing meteorological conditions (Konings et al., 2021). Vegetation browning can occur across a range of spatial scales, from localised patches to regional extents (Murthy and Bagchi, 2018; Liu et al., 2023a).

Vegetation dynamics can be evaluated through remote sensing (Lambert et al., 2013; Pan et al., 2018). In this context, satellites with varying spatial, spectral, and temporal resolutions offer distinct advantages for vegetation monitoring (Homolová et al., 2013). These offer diverse spectral bands, including visible and infrared wavelengths, making them effective tools for vegetation monitoring and assessment (Zeng et al., 2022). The Landsat and Sentinel satellite constellations, with their relatively high spatial resolution ($\leq$ 30 m), facilitates studies of vegetation at local to regional scales (Yang et al., 2012; Frampton et al., 2013; Schultz et al., 2016). In contrast, the Moderate Resolution Imaging Spectroradiometer (MODIS) satellites, with a coarser spatial resolution (250–1000 m), enable studies on a regional to global scale (Zhang et al., 2003, 2017).

Most studies address vegetation browning as a long-term process (Zhang et al., 2017; Pan et al., 2018), often associated with rainfall deficits or rising average temperatures linked to climate change (Liu et al., 2021, 2023a). However, short-term changes due to climate variability are also suggested to be influenced by climate change (Thornton et al., 2014), and may drive rapid vegetation declines (De Jong et al., 2012). In particular, drought severity has been recognised as a key disturbance capable of inducing rapid vegetation browning (Liu et al., 2023a,b). While trend analyses are commonly used to identify long-term changes, alternative methods can effectively characterise and monitor rapid browning events (Fang et al., 2018). Change detection algorithms, which account for both trends and short-term fluctuations, may therefore be suitable for tracing and studying sudden browning events (Wanyama et al., 2020).

When vegetation experiences stress, leading to a loss of vigour and greenness, these effects can be detected through vegetation indices such as the normalised difference vegetation index (NDVI) (Bannari et al., 1995; Chapungu et al., 2020). As vegetation degradation progresses, metabolic processes, including photosynthesis, may decline, eventually leading to a reductions in vegetation productivity (Letts et al., 2010; Takahashi et al., 2020). This deterioration can be expressed as reductions in leaf area index (LAI) and, in severe cases, a decrease in gross primary productivity (GPP) (Vicca et al., 2016; Jiang et al., 2021; Chen et al., 2021). However, once disturbance sources subside, vegetation can recover over the medium term. This recovery can serve as a proxy for evaluating vegetation's resilience and elasticity in response to stress, particularly in vegetation formations adapted to dry conditions (Liu et al., 2024).

Different vegetation characteristics and landscape attributes can significantly influence how vegetation responds to various disturbances (Frolking et al., 2009; Smith et al., 2014). For instance, solar radiation varies with slope aspect (Duffie et al., 2020), and steeper gradients are often associated with shallower soils (Liu et al., 2001), which can affect how vegetation responds to stresses such as severe droughts. Additionally, vegetation types vary in their resilience to degradation sources, with some more adapted to stress conditions, enabling differential responses to disturbances (Chelli-Chaabouni, 2013; Vicente-Serrano et al., 2013). Latitudinal and altitudinal gradients, which influence rainfall patterns (Fuentes et al., 2024b), also introduce variations that affect drought propagation and its impact on vegetation.

Consequently, the primary objective of this research is to assess the relationship between vegetation browning, ecosystem resilience and drought propagation in central Chile using change detection algorithms to track vegetation responses to rapid and severe dry conditions. This analysis incorporates MODIS time series for NDVI, LAI, and GPP to track drought progression. We examine the timing and magnitude of changes in vegetation in relation to latitudinal, topographic and vegetation differences. Furthermore, vegetation recovery extents, the lag time from disturbance events, and shifts in temporal autocorrelation of vegetation index time series are also evaluated as proxies for resilience. This study focuses on highly heterogeneous vegetation systems in central Chile, recognised as a biodiversity hotspot (Myers et al., 2000), which has experienced widespread browning linked to severe droughts (Miranda et al., 2020, 2023). However, browning assessments in this region have primarily relied on long-term trend analysis (Miranda et al., 2020) or time series of annual vegetation index anomalies (Miranda et al., 2023), and studies on vegetation recovery following browning events are still absent.

2. Materials and methods

2.1. Study region

This study was conducted in Chile, between the Valparaiso and O'Higgins regions (latitudes −34.98 – −32.02) in an area of 47,721 km^2, where widespread browning associated with prolonged drought conditions has been reported (Miranda et al., 2020, 2023; Fuentes et al., 2024a). The northern part of the study area has a semiarid climate (Köppen–Geiger *BSk*), while hot and warm summer Mediterranean climates dominate most of the region (Koppen–Geiger *Csa* and *Csb*). Eastward, towards the Andes, the climate transitions into cold-summer Mediterranean and Tundra climates (Köppen–Geiger *Csc* and *ET*, respectively) (Beck et al., 2018).

Elevation, annual rainfall and mean annual temperatures in the study region are shown in Fig. 1. Rainfall, which occurs predominantly in winter, follows a latitudinal gradient with higher precipitation levels towards the south. The region contains diverse vegetation formations (Luebert and Pliscoff, 2022), being dominated by sclerophyllous forests and shrubs, and thorny forests. These vegetation types display adaptive traits that enhance tolerance to water deficits (Yin and Bauerle, 2017) and reflect adaptations to the latitudinal gradient.

A persistent "megadrought" has impacted the study region since 2010 (Garreaud et al., 2020). However, recent years have seen a slight offset in these water deficit conditions due to normal or above-average annual rainfall, particularly during 2023–2024, driven by the warm phase of El Niño Southern Oscillation (ENSO). The effects of this prolonged drought and recovery scenarios remain an active area of local research.

2.2. Remote sensing datasets and pre-processing

In this study, we used data from the MODIS Terra satellite to monitor vegetation changes associated with severe droughts as a proxy for evaluating rapid browning processes and vegetation recovery. Specifically, we selected three products: (i) NDVI band from the Terra Vegetation Indices (MOD13A1) with a temporal resolution of 16 days; (ii) the LAI band from the Terral Leaf Area Index/FPAR (MOD15A2H) with an 8-day temporal resolution; and (iii) the GPP band from the Penman–Monteith–Leuning evapotranspiration dataset (PML_V2) with an 8-day temporal resolution. To ensure data quality, pixels with clouds or snow/ice in the NDVI collection were masked out based on the quality band information.

NDVI, which calculates the normalised difference between red and near infrared wavelength bands, is widely used as a proxy for monitoring vegetation vigour (Al-Nasrawi et al., 2021). LAI represents the leaf area per unit of ground surface and is derived from surface reflectance data using a radiative transfer model and a look-up table (Myneni and Park, 2015). GPP, which estimates the amount of carbon fixed by vegetation through photosynthesis, is estimated through the PML model. This model integrates evapotranspiration via canopy conductance and utilises reflectance and meteorological data for accurate estimation (Zhang et al., 2019).

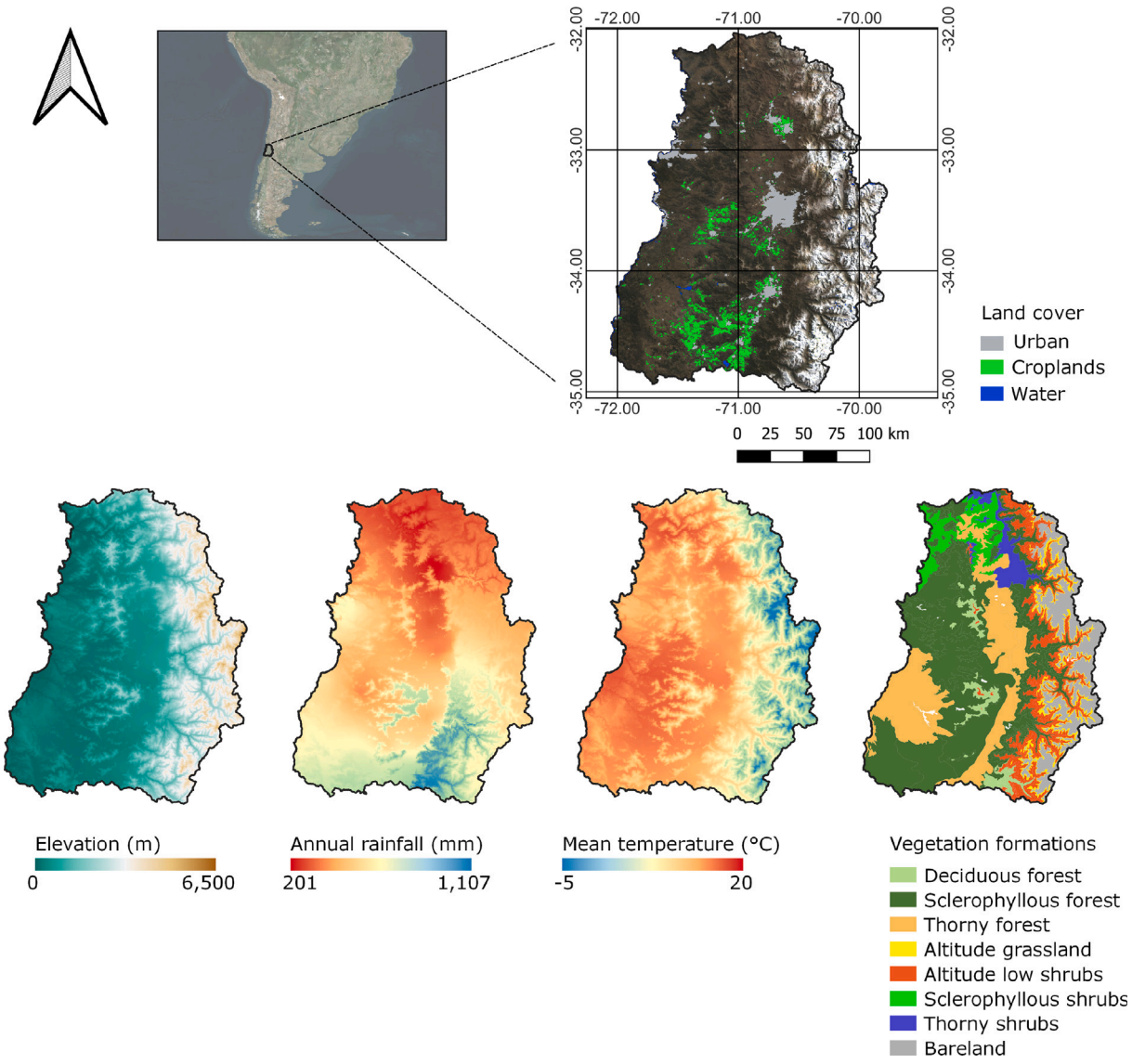

Fig. 1. Study area showing physiographic characteristics: elevation, annual rainfall, mean temperature, and vegetation formations. Additionally, urban and agricultural areas which are significant in the region are also shown. Annual rainfall and mean temperatures were obtained from the WorldClim Climatology v1 dataset (Hijmans et al., 2005).

Table 1
Sources of data included in this study.

Dataset	Variable	Spatial resolution	Temporal resolution	Operation period	Source
MOD13A1	NDVI	500 m	16-days	2001–now	Didan et al. (2015)
MOD15A2H	LAI	500 m	8-days	2001–now	Myneni and Park (2015)
PML_V2	GPP	500 m	8-days	2001–2023	Zhang et al. (2019)
Fire_cci v5.1	Fire	250 m	monthly	2001–2020	Lizundia-Loiola et al. (2020)
MCD12Q1	Land Cover	500 m	annual	2001–2023	Friedl and Sulla-Menashe (2019)
MERIT DEM	DEM	90 m	–	–	Yamazaki et al. (2017)
CR2/DGA/DMC	Rainfall	–	monthly	variable	https://www.cr2.cl/

Additionally, various datasets were used to mask out other sources of vegetation degradation (Table 1). Fire data from the MODIS Fire_cci Burned Area Pixel Product v 5.1 from the European Space Agency (ESA) Fire Climate Change Initiative (Fire_cci), was aggregated over time (Lizundia-Loiola et al., 2020). To ensure pixel selection, a mask was created based on fire confidence levels, excluding pixels with a confidence level above 50% (indicating likely fire impact). Land cover data from the 2019 MODIS Land Cover Type dataset (MCD12Q1) following the Annual International Geosphere-Biosphere Programme classification was also used (Friedl and Sulla-Menashe, 2019); pixels not classified as natural vegetation were masked out. Additionally, deforestation pixels from Fuentes et al. (2024a) and the Global Forest Watch platform (Watch, 2002) were excluded to isolate drought-driven vegetation changes by removing areas where deforestation was likely a confounding factor.

Other remote sensing data sources included the Multi-Error-Removed Improved Terrain (MERIT) digital elevation model (DEM) with a 3-arc-second spatial resolution, from which slope and aspect were derived. Vegetation formations were obtained from Luebert and Pliscoff (2022). Data acquisition, processing, and analysis were conducted using Google Earth Engine (Gorelick et al., 2017) and Google Colab. All gridded

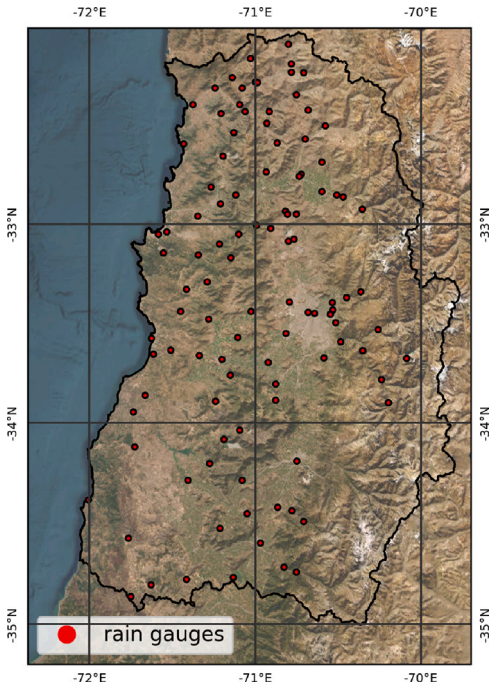

Fig. 2. Rain gauges used in this study, with data at monthly temporal resolution, installed and managed by the Water Resources Directorate (DGA) and the Meteorological Directorate of Chile (DMC).

data sources were reprojected to match the MODIS spatial resolution (500 m).

2.3. Ancillary datasets

Monthly rainfall data from meteorological stations was obtained from the Centre for Climate and Resilience Research (CR2) and filtered based on the study region from 1980 to 2020. This was supplemented with recent records (post-2020) from the Water Resources Directorate (*Dirección General de Aguas*; DGA) and the Meteorological Directorate of Chile (*Dirección Meteorológica de Chile*; DMC). Stations were further filtered to include only those with at least 20 years of data, resulting in 106 rainfall gauges (Fig. 2). The Standardised Precipitation Index (SPI) was calculated monthly using the calendar year from the rainfall series using a three-month window, as it reduces short-term noise while still capturing the short-term impacts of drought conditions (McKee et al., 1993; Guenang and Kamga, 2014). Additionally, monthly rasters of SPI were generated by applying a radial basis function (RBF) interpolation with a linear function.

The reference dataset from Fuentes et al. (2024a), comprising 91 polygons representing areas with vegetation browning due to droughts and 83 polygons indicating stable vegetation, was used to fine-tune the classification of vegetation browning in this study. This dataset was developed by visually interpreting temporal series of high-resolution images available in Google Earth Pro, with polygons drawn to represent various known sources of vegetation change.

2.4. Change detection algorithm

We estimated abrupt changes in vegetation index time series using the Continuous Change Detection and Classification (CCDC) algorithm as a segmentation method implemented in Google Earth Engine, which decomposes time series data into intra-annual, inter-annual, and structural changes. We selected CCDC because it enables pixel-wise time series analysis and the detection of short-term vegetation changes, including both degradation and recovery. Additionally, Fuentes et al. (2024a) compared CCDC with other algorithms and found that it provides a fast response and performs well in tracking different vegetation changes. CCDC fits ordinary least squares (OLS) regressions, tracking deviations between observations and predictions to detect changes using time-stamped bivariate/multivariate data. Originally developed to monitor land cover changes (Zhu and Woodcock, 2014), the algorithm assumes time series with inherent seasonality, trends, and breaks, estimating coefficients through OLS and fitting harmonic functions as follows:

$$\hat{\rho}(i,x)_{OLS} = a_{0,i} + a_{1,i}cos(\frac{2\pi}{T}x) + b_{1,i}sin(\frac{2\pi}{T}x) + c_{1,i}x \quad (1)$$

in this case x is limited to the boundaries:

$$\tau^*_{k-1} < x \leq \tau^*_k \quad (2)$$

being $\hat{\rho}(i,x)_{OLS}$ the estimated value of the time series, x the day of the calendar year; i the dimensions of the time series (number of bands); T the number of days per year; while $a_{0,i}$; $a_{1,i}, b_{1,i}$; and $c_{1,i}$ are the overall (mean; a_0), intra-annual change (seasonal; a_1, b_1), and inter-annual (trend; c_1) change coefficients for the i band, respectively; and τ^*_k are the kth break points.

CCDC assesses differences between predictions and observations by using the root mean square error (RMSE) within a defined time window in single-band or multi-band images:

$$\frac{1}{k}\sum_{i=1}^{k}\frac{|\rho(i,x) - \hat{\rho}(i,x)_{OLS}|}{n \times RMSE_i} > 1(z \text{ consecutive times}) \quad (3)$$

where k corresponds to the number of bands, n is an RMSE-multiplying factor for change detection (set to 3 in this case), and z indicates the required consecutive observations where errors exceed n times the RMSE to confirm a change. We used the change dates and magnitudes retrieved by CCDC to evaluate vegetation browning caused by severe meteorological water deficits and its subsequent recovery. Change magnitudes were calculated as the difference between the average NDVI values in stable periods before and after a detected change, capturing the impact of individual drought-induced shifts in vegetation. While these magnitudes are not cumulative in a strict sense, they may reflect the cumulative stress imposed by drought conditions over time. Up to five structural changes per pixel were stored and analysed, ensuring a detailed assessment of vegetation response to prolonged water deficits.

2.5. Evaluation of changes

The CCDC algorithm was applied with the parameter z set to 5, and various chi-square probability thresholds, ranging from 0.9 to 0.99, were tested to optimise detection performance. The CCDC results were then compared with the change and stable polygons from the reference dataset of Fuentes et al. (2024a), with examples shown in Fig. 3. To evaluate the accuracy of the detected changes, we considered any CCDC-detected change within a change polygon as a valid change, while correct stable regions were defined as those where no CCDC changes were detected within stable reference polygons.

The performance of vegetation change detection was assessed using various metrics derived from the NDVI image collection using the adapted reference dataset. Parameters optimised for detection performance using the NDVI collection were applied to other collections, assuming favourable results. The performance metrics evaluated included overall accuracy (OA), F1-score, and Cohen's Kappa (kappa) coefficient. The OA metric represents the proportion of correctly classified samples relative to the total sample size; the F1-score is particularly useful when the data is imbalanced and represents the harmonic mean between precision and recall; the Kappa coefficient, which is more conservative, indicates the level of agreement between observations and classifications, adjusting for chance agreement (Olofsson et al., 2014). Additionally, the area under the curve (AUC) for Receiver Operating

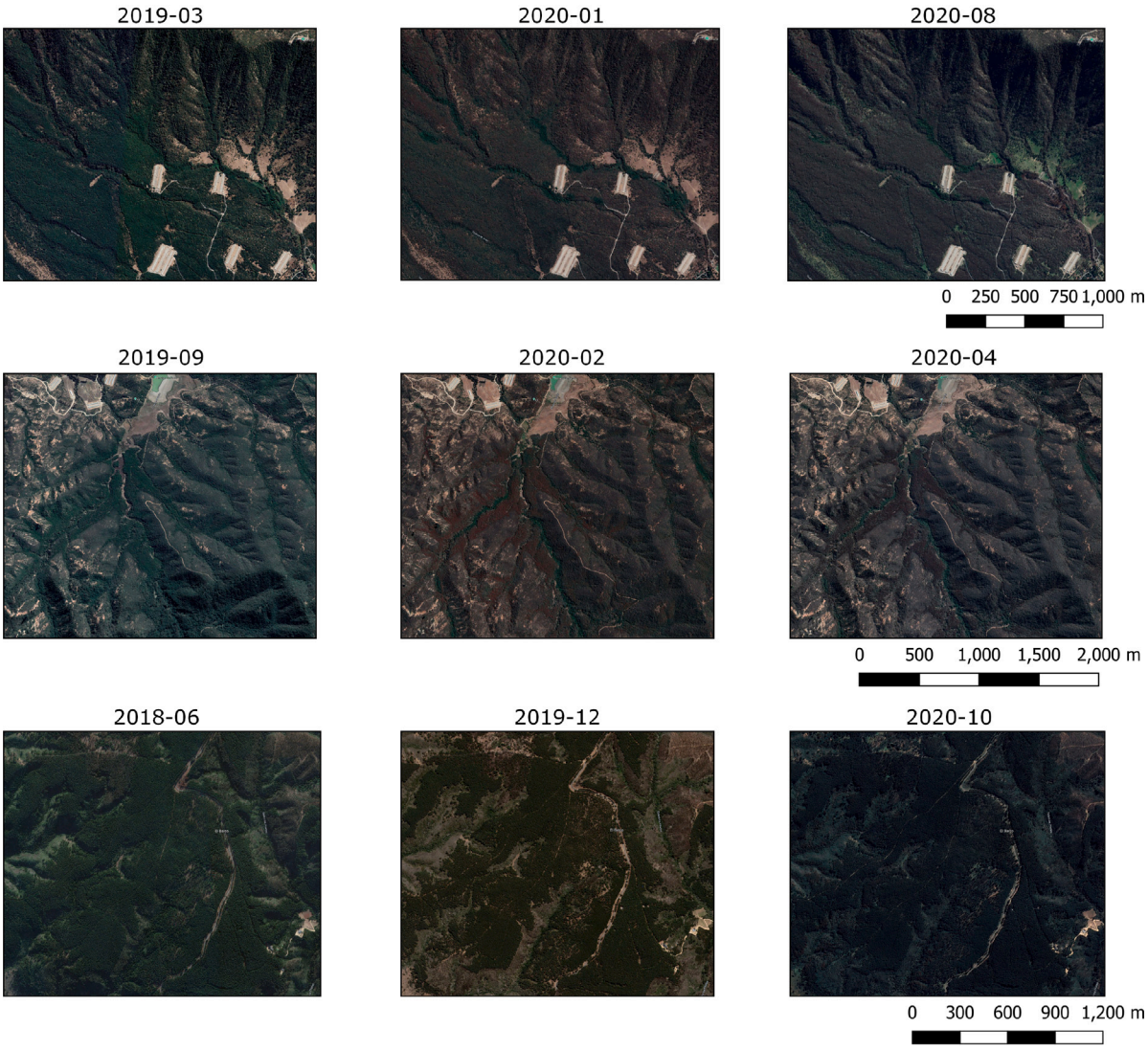

Fig. 3. Example areas containing series of three dates with vegetation affected by drought (first two row panels) and stable vegetation (last row panel).

Characteristic (ROC) curves was calculated using the trapezoidal rule. These metrics are calculated as:

$$OA = \frac{tp + tn}{tp + fp + tn + fn} \tag{4}$$

$$kappa = \frac{P_o - P_e}{1 - P_e} \tag{5}$$

$$F1 = 2 \times \frac{precision \times recall}{precision + recall} \tag{6}$$

being tp, fp, tn, fn, P_o, and P_e true positive, false negative, true negative, false negative, the probabilities of real agreement, and probabilities of agreement due to chance, respectively. Additionally, precision and recall can be estimated as:

$$precision = \frac{tp}{tp + fp} \tag{7}$$

$$recall = \frac{tp}{tp + fn} \tag{8}$$

These metrics guided the selection of the chi-square threshold for the CCDC algorithm to enhance detection performance.

2.6. Vegetation browning and resilience assessment

Change dates and magnitudes were filtered in a first stage to include only negative changes (negative change magnitudes), representing vegetation browning. Given the extensive changes occurring as a response to meteorological water deficits between the second half of 2019 and the end of 2020, browning changes were constrained to this period. The time lag in vegetation response was calculated as the difference between the onset of meteorological droughts, identified when SPI values fall below −1, and the NDVI-based vegetation change dates. Additionally, vegetation response propagation was further assessed by analysing GPP and LAI change dates, which indicate vegetation productivity reduction. The cumulative effects of drought were evaluated through the change magnitudes of NDVI, GPP, and LAI, which quantify the severity of vegetation browning and productivity losses over time. The spatial extent of these vegetation changes was also estimated.

Vegetation changes were analysed to evaluate particular vulnerabilities, focusing on latitudinal gradients, topographic features, and vegetation types. The latitudinal gradient in Chile significantly influences rainfall patterns and vegetation dynamics (Fuentes et al., 2024b), potentially affecting the timing and magnitude of vegetation changes. Topographic features, including slope aspect categorised into octants, and vegetation types, such as formations described by Luebert and Pliscoff (2022) and land cover classes from Friedl and Sulla-Menashe (2019) were also considered to explore vegetation vulnerability to water deficits. Differences in the magnitude and timing of changes in these categories were assessed to provide insights into the severity of water deficits and the lag in drought response. Statistical analysis included analysis of variance or the non-parametric Kruskal Wallis test

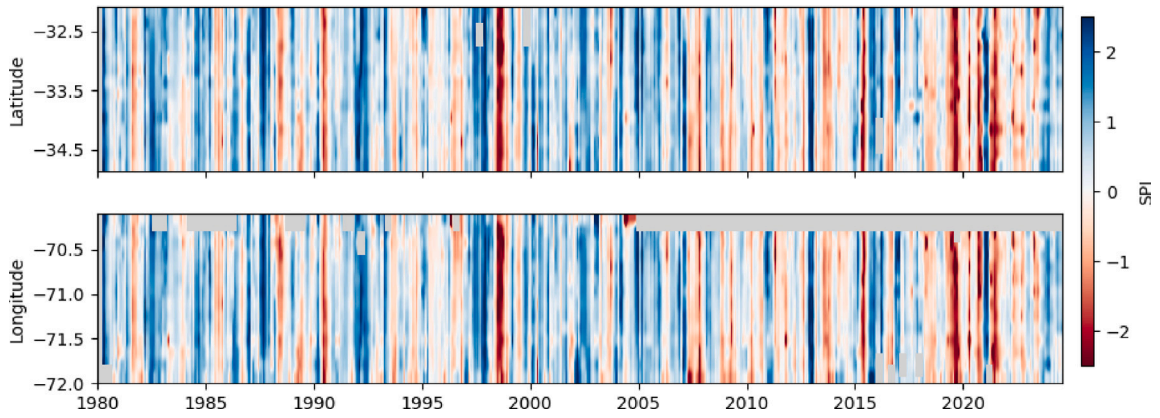

Fig. 4. Heat map of SPI in the study area, showing temporal variations in dry and wet conditions.

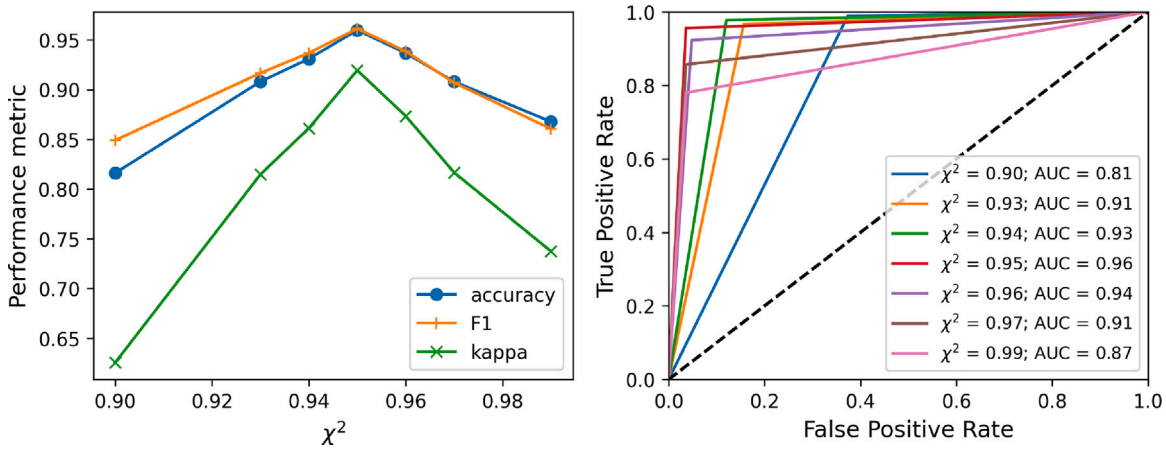

Fig. 5. Performance metrics calculated from detection changes using reference polygons of stable and drought affected vegetation depending on the chi-square probability used in the CCDC.

to assess possible spatial patterns exacerbating browning intensification. Post-hoc comparisons employed Dunn's multiple comparison test with a Bonferroni adjustment (Glantz et al., 2002). A p-value < 0.05 was considered indicative of statistically significant differences across categories.

Subsequently, vegetation regrowth was assessed by examining positive changes in magnitude following browning events in pixels that experienced significant declines in vegetation. Vegetation regrowth was analysed from 2021 onward, as severe water deficits subsided afterwards, allowing for the evaluation of regrowth extent, magnitude, and lagged response as key indicators of resilience (Liu et al., 2024). Beyond regrowth metrics identified through change detection algorithms, resilience was further examined by assessing long-term shifts in vegetation stability, following Forzieri et al. (2022). Specifically, we analysed changes in temporal autocorrelation (TAC) of kNDVI:

$$kNDVI = tanh(NDVI^2) \tag{9}$$

kNDVI serves as a proxy for vegetation productivity and is particularly suited for evaluating long-term shifts in ecosystem stability. This transformation enhances sensitivity to structural vegetation changes and may facilitate the detection of resilience patterns over time. TAC changes in kNDVI were analysed for two periods,2000–2012 and 2013–2024.

For the TAC analysis, images were first converted from NDVI to kNDVI, then de-seasonalised by subtracting mean kNDVI values aggregated by the day of the year. The time series were further detrended using ordinary least squares regression. TAC was calculated at the 1-lag for the periods 2001–2012 and 2013–2024, with these periods chosen to capture distinct phases in the data. The earlier period (2001–2012) represents a baseline or pre-disturbance period, while the later period (2013–2024) reflects potential changes associated with climate-related stressors, land use, or other factors. Changes in TAC, quantified as δTAC by subtracting TAC values of the two periods, allow for the analysis of shifts in vegetation resilience over time. Land cover classes including agricultural lands were masked out in this analysis. An increase in TAC (δTAC > 0) indicates a decline in forest resilience because it reflects the system's reduced ability to recover from disturbances, a phenomenon known as critical slowing down (Weinans et al., 2021). This suggests that the ecosystem is becoming less stable and more vulnerable to tipping points or regime shifts under environmental stressors (Forzieri et al., 2022).

3. Results

3.1. Meteorological drought and change detection validation

Fig. 4 presents a heat map of drought conditions across the study region, highlighting that dry conditions have dominated a significant portion of the territory over the past decade. Notably, pronounced rainfall deficits occurred in mid-2019 and extended through 2020. In contrast, wetter conditions emerged in 2023, partially attributed to a strong El Niño event (Lian et al., 2023).

The performance of the NDVI-based vegetation change detection using reference polygons is shown in Fig. 5. Setting the chi-square

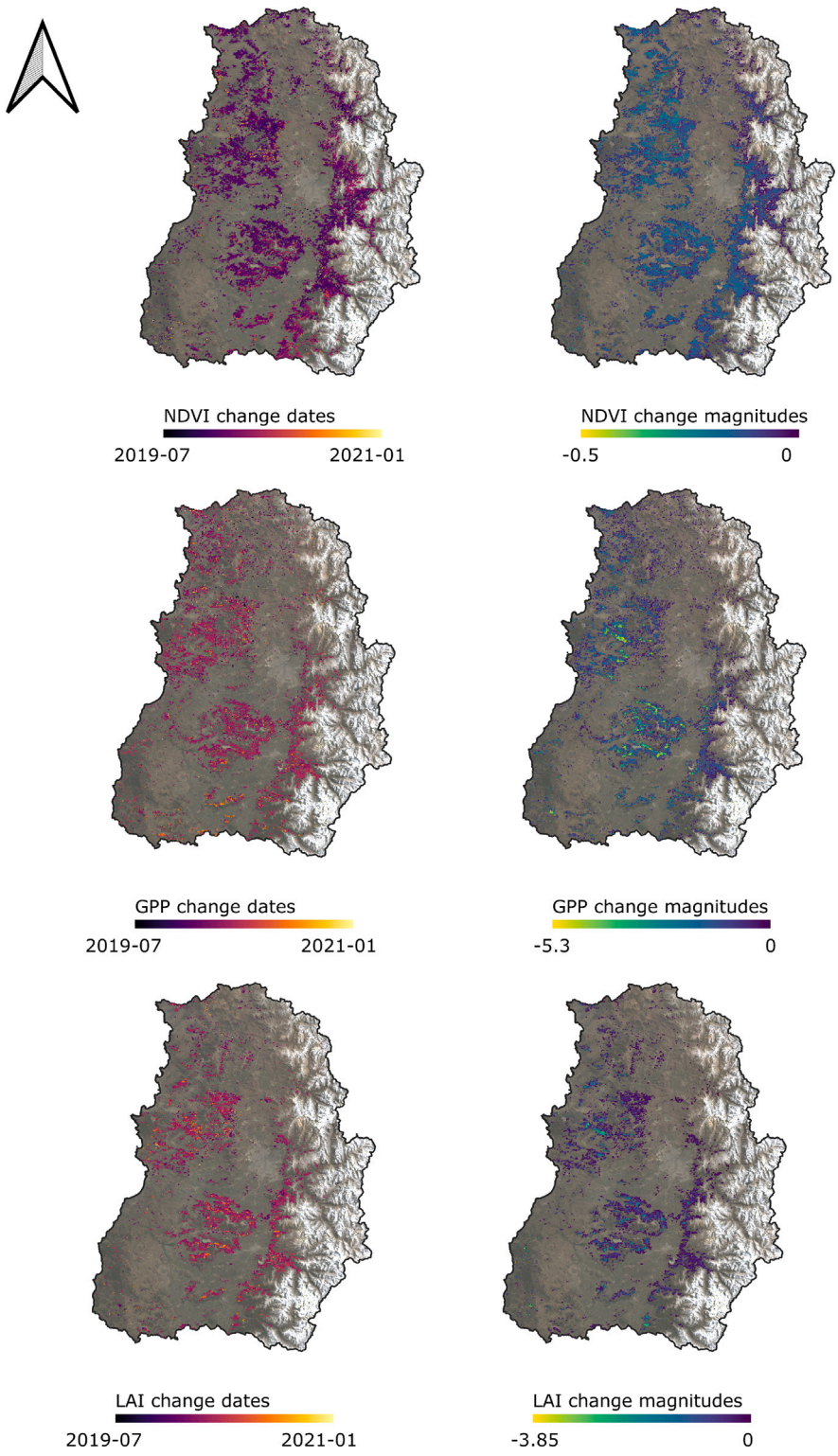

Fig. 6. Vegetation changes for NDVI (top panel), GPP (middle panel) and LAI (bottom panel) MODIS image collections using CCDC, showing change dates and change magnitudes.

probability to 0.95 in the CCDC algorithm yielded the best results, with an OA of 0.95, a F1-score of 0.96, a kappa of 0.91, and an AUC of 0.96. This chi-square probability was subsequently applied to additional analyses. However, performance declined when evaluating against GPP vegetation changes, with results showing an OA of 0.87, a F1-score of 0.86, a kappa of 0.75, and an AUC of 0.88, which was deemed sufficient for further analysis.

3.2. Tracking drought propagation in vegetation: browning and recovery

Vegetation changes are shown in Fig. 6, with NDVI changes in the top panel, GPP in the middle panel, and LAI in the bottom panel. The spatial discontinuity of drought-induced vegetation changes is expected due to multiple interacting factors such as topography, vegetation types, and land cover characteristics (Hollunder et al., 2021), leading to a heterogeneous pattern of browning across the landscape. NDVI

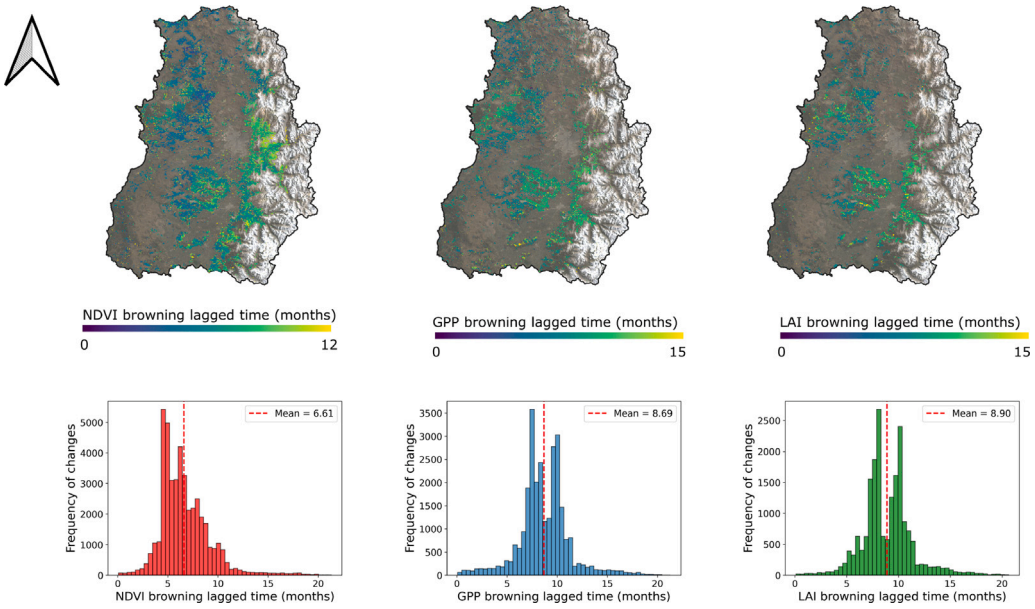

Fig. 7. Spatial distribution of drought lagged response times for vegetation indices (NDVI, GPP, and LAI) (top row) and corresponding histograms of lag times (bottom row).

changes cover the largest area (9200 km^2), followed by GPP (5697 km^2) and LAI (4026 km^2). This indicates that not all reductions in vegetation vigour lead to significant productivity loss. Additionally, a lagged response is observed, with structural changes in LAI and GPP following NDVI changes (Fig. 7).

Time series of NDVI for pixels experiencing changes across different latitudes are shown in Fig. 8, while GPP are LAI time series are in the Supplementary Materials (Figures S1 and S2, respectively). NDVI exhibits greater seasonal fluctuation and higher interquartile ranges (IQR) in northern regions. In contrast, GPP and LAI show increased IQR in southern regions with large deviation, possible due to the impact on deciduous forests and greater vegetation variability in the LAI series. Change dates in the NDVI series correspond to a sharp drop below prior minimum values, followed by a gradual recovery trend in subsequent years. GPP and LAI changes are also evident, though less pronounced compared to NDVI.

Vegetation recovery, expressed as positive changes in vegetation indices detected in pixels affected by browning after 2021, is in Fig. 9. The extent of these recovery changes is significantly smaller than the browning extent, indicating a partial recovery of vegetation that has not yet returned to pre-drought conditions. Specifically, only 23.9%, 12.7%, and 21% of the areas affected by browning in terms of NDVI, GPP, and LAI, respectively, show signs of recovery. Fig. 10 shows the spatial distribution of vegetation recovery lag times, measured from the onset of vegetation drought response (browning) detected through NDVI. The histograms indicate that LAI generally has the longest recovery time, while NDVI recovers slightly faster on average. The observed spatial variability suggests that ecosystem resilience differs across the region, likely influenced by vegetation type and local environmental conditions.

Histograms of change dates and magnitudes for the study region are in Fig. 11. Vegetation browning is represented in red, indicating negative change magnitudes, while vegetation recovering is shown in blue, corresponding to positive change magnitudes. Browning events are concentrated within shorter time frames compared to vegetation recovery, which show a more prolonged and disperse lag in response. While changes in vegetation indices exhibit similar patterns, significantly more NDVI changes occur and tend to peak on average about two months earlier than GPP and LAI changes (approximately 60 days earlier). The lag between rainfall deficits, marked by the onset of moderate drought conditions, and negative changes in NDVI averages around 6.6 months (approximately 200 days; Fig. 7). In contrast, negative changes in GPP and LAI appear on average about 8.7 months after rainfall deficits (approximately 260 days). For vegetation recovery, responses following the onset of vegetation browning occur on average 3.3, 3.6, and 3.9 years later for NDVI, GPP, and LAI, respectively.

Change magnitudes vary depending on the normal range of each vegetation index: NDVI typically ranges between 0 and 1 for vegetation, GPP between 0 and 39 gC m^{-2} d^{-1}, and LAI between 0 and around 10. Negative change magnitudes, associated with browning, decrease in frequency as magnitude decreases, whereas positive change magnitudes, associated with recovery, are more evenly distributed. Additionally, violin plots of change magnitudes by date range are displayed in Fig. 12. Browning-related change magnitudes (A) show a relatively uniform pattern across vegetation indices, while recovery-related magnitudes exhibit contrasting behaviours. NDVI recovery magnitudes tend to increase over time, whereas GPP and LAI recovery magnitudes show high variability.

3.3. Browning and its interrelation with other variables

Fig. 13 shows the amount and distribution of browning pixels according to latitudinal distribution (i.e., proxy for water availability), topographic aspect (i.e., proxy for radiation and water availability), vegetation formation, and land cover type. Significant differences were observed in the dates and magnitudes of vegetation changes across latitudes when using different indices (Fig. 13 top panel; Supplementary Materials, Tables S1- S6). For example, we observed an NDVI trend of delayed change dates southward, indicating a slower propagation of drought effects towards southern regions. In contrast, other vegetation indices such as GPP and LAI appear less sensitive to latitudinal variations. In terms of change magnitudes, NDVI exhibits greater data dispersion compared to GPP and LAI, although all indices show considerable fluctuation across latitudes. It is important to note that changes in NDVI do not always correspond with changes in LAI, highlighting that shifts in vegetation vigour (as indicated by NDVI) do not necessarily reflect alterations in productivity.

Significant differences were also identified across aspect octants (second row panel of Fig. 13; Supplementary Materials, Tables S7–S13). Notably, greater differences in change dates across aspect octants were found when evaluating productivity (LAI and GPP) rather than vegetation vigour (NDVI). For vegetation productivity, change dates tended to

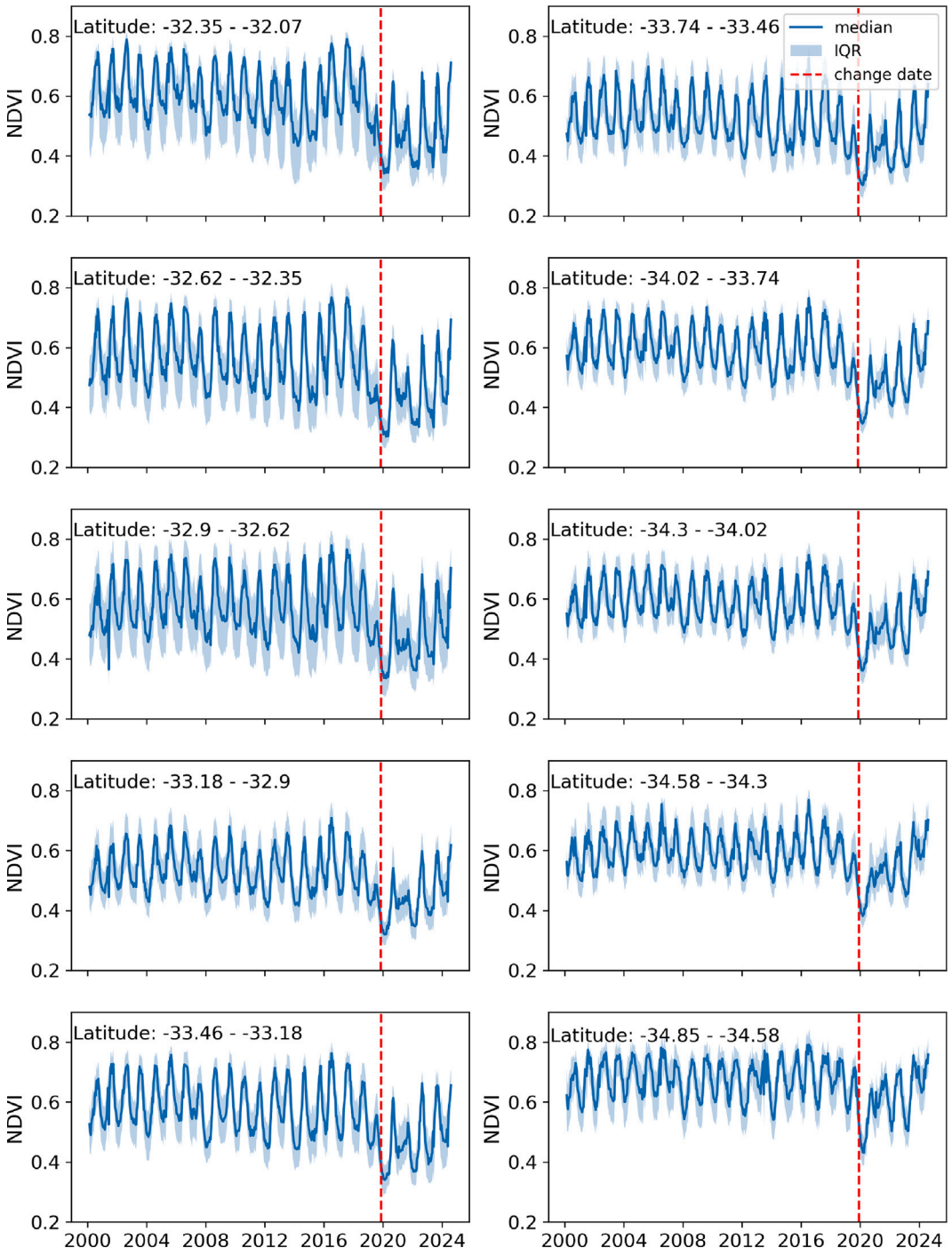

Fig. 8. NDVI time series with median values (solid blue line) and interquartile ranges (IQR; blue shading) across latitudes. The mean change date detected by the algorithm is shown as a dashed red line. (For interpretation of the references to colour in this figure legend, the reader is referred to the web version of this article.)

group into two main clusters: one comprising the western, northwestern, northern, and northeastern octants, and another with the eastern, southeastern, southern, and southwestern octants, where changes occurred later. A leftward shift in normalised change magnitudes for NDVI was observed in the southern, southeastern, and southwestern octants, while a rightward shift was noted in the northern, northwestern, and western octants. In contrast, LAI showed fewer differences across octants, with most distinctions occurring specifically in the western octant compared to other directions.

Most vegetation changes occur within Sclerophyllous forest formations (third row panel if Fig. 13), though there are significant differences across vegetation types (Supplementary materials, Tables S13–17). Changes appear earlier in thorny shrublands and later in deciduous forests and Andean shrublands. Interestingly, deciduous and sclerophyllous forests show similar patterns in vegetation productivity across change dates. The largest positive shift in change magnitude occurs in Andean shrublands, while the largest negative shift is observed in Sclerophyllous forests.

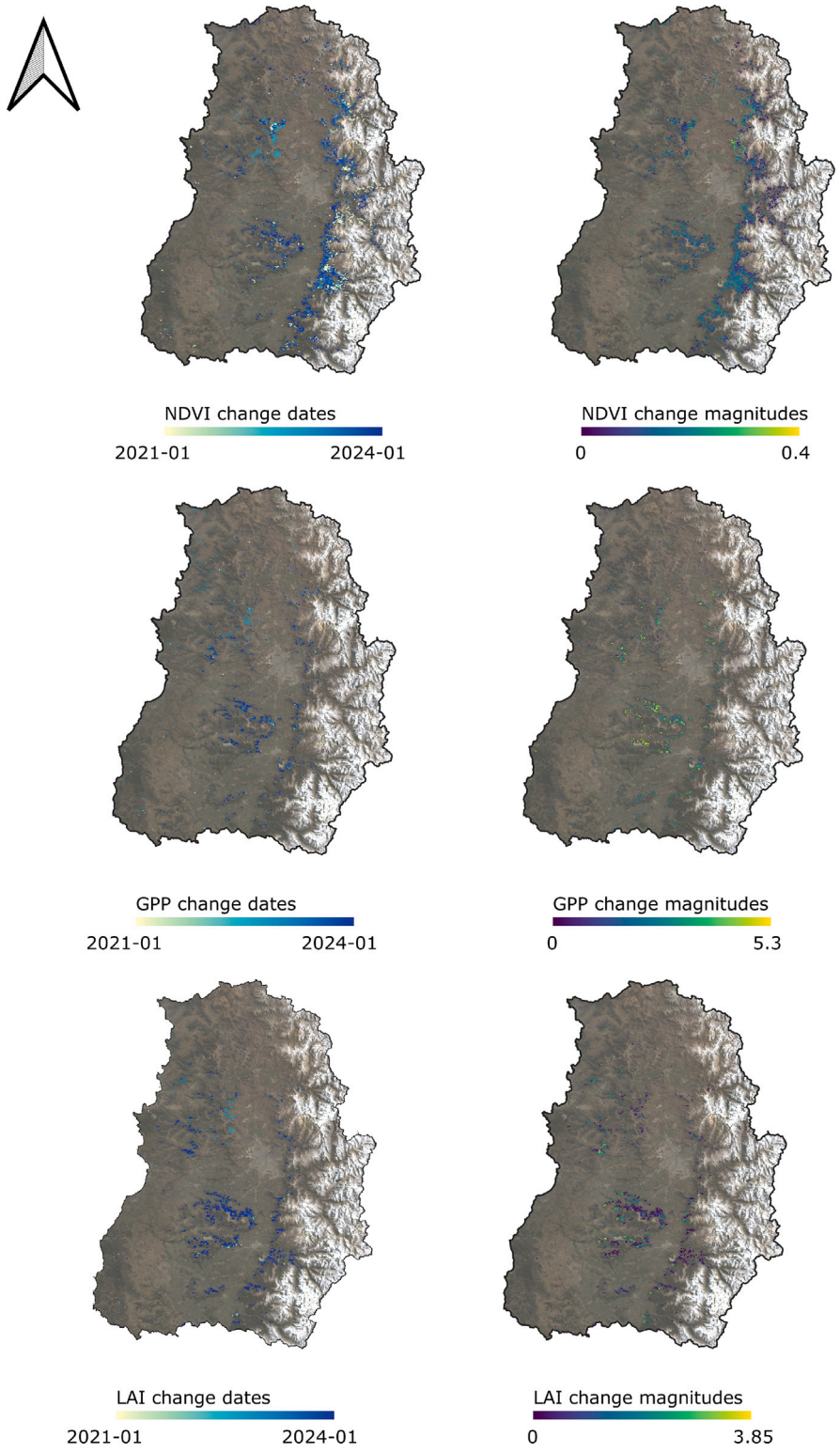

Fig. 9. Recovery in vegetation changes for NDVI (top panel), GPP (middle panel), and LAI (bottom panel) MODIS image collections using CCDC, showing dates of change and change magnitudes.

The bottom panel of Fig. 13 illustrates changes across land cover types. The majority of changes occur in savanna and woody savanna classes, followed by grasslands. While NDVI change dates vary across land cover classes, productivity changes (GPP and LAI) in forests and woody savanna occur later than in herbaceous or shrubland classes. In terms of change magnitudes, both forest classes tend to cluster together,

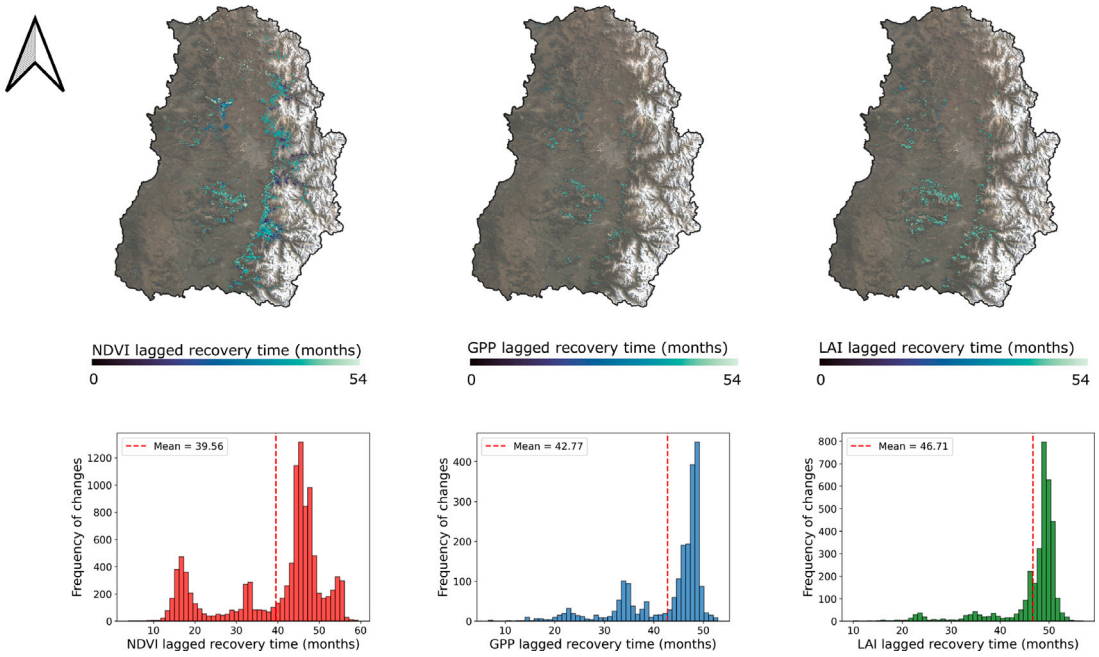

Fig. 10. Spatial distribution of recovery lagged response times for vegetation indices (NDVI, GPP, and LAI) (top row) and their corresponding histograms (bottom row), showing the frequency of lag times in months.

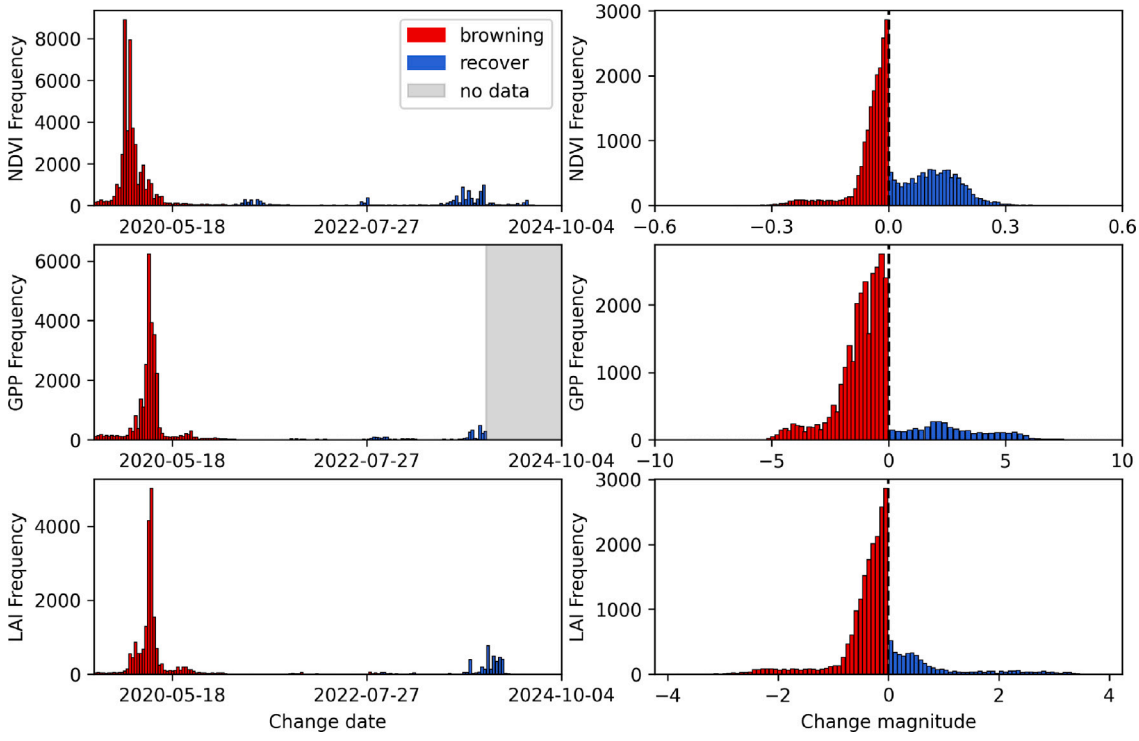

Fig. 11. Histograms of dates and magnitudes of changes for NDVI (top panel), GPP (middle panel), and LAI (bottom panel) collections for vegetation browning (red) and recovery (blue). (For interpretation of the references to colour in this figure legend, the reader is referred to the web version of this article.)

displaying a strong shift towards negative normalised magnitudes. This indicates that these forest classes experience larger change magnitudes relative to their mean values.

3.4. Shift in vegetation resilience

The previous sections analysed how drought conditions propagated into vegetation, leading to browning events and subsequent recovery. However, an equally critical aspect is whether disturbances, including meteorological conditions, have induced long-term shifts in vegetation resilience. To assess this, we evaluate changes in kNDVI temporal autocorrelation (TAC) across two periods as a proxy for vegetation resilience (see Section 2.6).

Fig. 14 illustrates the spatial distribution of δTAC (left) and its probability density (right). A large portion of the study area shows a positive shift in δTAC between the period 2000–2012 and 2013–2024,

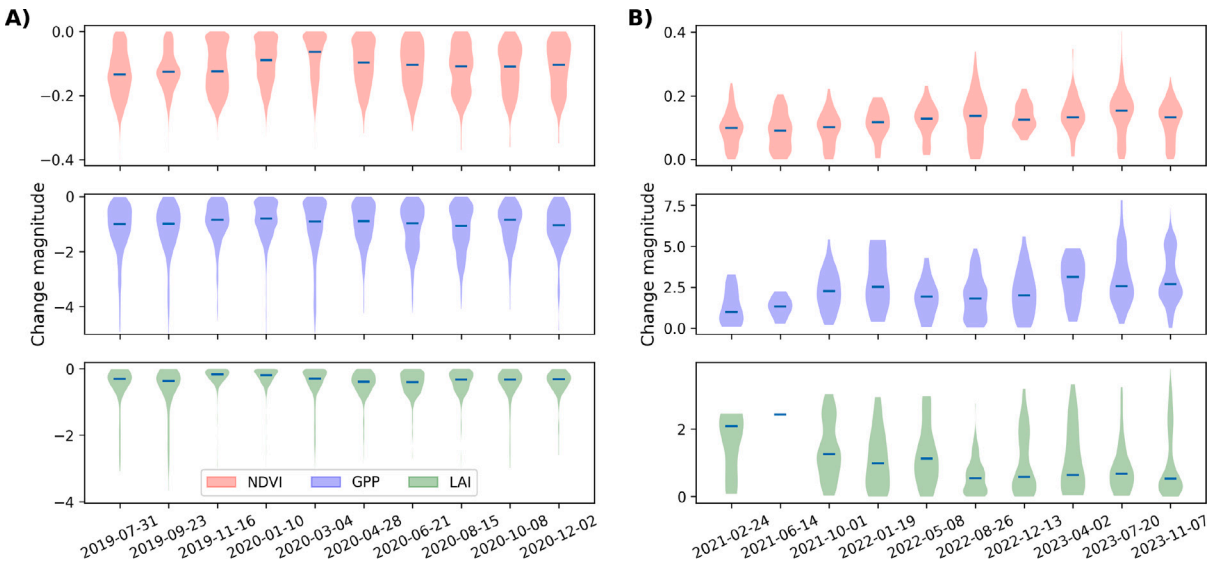

Fig. 12. Violin plots of change magnitudes for different date ranges for NDVI, GPP, and LAI, showing vegetation browning (A) and recovery (B).

indicating a general decrease in vegetation resilience. This difference is more pronounced in areas experiencing vegetation changes. The probability density plot further highlights this shift towards positive values, reinforcing the observed reduction in vegetation resilience across the region. Overall, 87.2% of the pixels display a positive shift, while only 12.7% show a negative shift, predominantly in the southwest region, where forestry activities are more prevalent and where large fires took place in 2017 (Bowman et al., 2019).

4. Discussion

4.1. Vegetation browning and change detection algorithms as proxies for drought propagation assessment

One of the most commons approaches to studying drought propagation involves the use standardised indices (Zargar et al., 2011; Zhang et al., 2022). In vegetation systems, this approach is often implemented through the standardisation of NDVI or other vegetation indices (Peters et al., 2002). The lagged response of vegetation or agricultural systems to atmospheric conditions has typically been studied by analysing the onset of deficit conditions (Zhang et al., 2022). In vegetation, this often involves using standardised indices similar to SPI, where drought conditions are assumed to begin when the standardised vegetation index falls below −1 (Li et al., 2020); the lag between signals is then calculated as the difference in onset times. Another method for assessing vegetation's lagged response involves calculating the time lag at which maximum autocorrelation occurs between standardised meteorological and vegetation indices (Fuentes et al., 2022). Similarly, the extent of drought impact on vegetation or agricultural systems is often determined using the same methodologies.

In this study, change detection using the CCDC algorithm proved to be a valuable tool for tracking drought propagation through vegetation browning, offering an alternatively to conventional methods and algorithms (De Jong et al., 2012). This approach can be applied not only to assess the spatial extent of vegetation affected by drought but also to evaluate vegetation's lagged response to meteorological drought and the magnitude of change in impacted areas. However, to accurately detect drought-specific signals and avoid confounding effects from other forms of vegetation degradation, additional steps may be required to isolate changes associated solely with drought impacts (Fuentes et al., 2024a).

One drawback of change detection methodologies is the latency in detecting changes, as most algorithms require a set of observations rather than a single record to define a change, thus reducing potential artefacts and outliers (Zhu et al., 2020). This delay, however, depends on the specific algorithm and the temporal resolution of the data used (Bullock et al., 2022). For example, Fuentes et al. (2024a) found that the CCDC algorithm performed well in terms of both accuracy and the temporal lag between disturbances and change detection using Landsat images, though a minimum lag of two months was still required to detect 50% of changes. In remote sensing, latency also varies according to the satellite used, due to differences in revisit times (Francini et al., 2020). Consequently, the more frequent the image acquisition, the faster the potential for change detection (Zhu, 2017). Although algorithm parameters can help to mitigate these delays, it is essential to balance detection speed with accuracy to minimise false alarms. This balance ultimately depends on the specific processes being studied and the decision-making context (Bullock et al., 2022).

Image spatial resolution is also an important factor in change detection analysis (Hammer et al., 2014; Francini et al., 2020). Given the widespread browning in the studied region, the moderate resolution provided by MODIS is appropriate for tracking these changes. However, for processes occurring at finer scales or for accurately determining the extent of these processes, higher-resolution data sources may be necessary (Morton et al., 2005). Additionally, high-resolution imagery can better capture the small-scale factors that influence drought propagation, which often vary significantly across the landscape. Therefore, given the differences in spatial scales it may be valuable to explore multi-scale analyses to study micro-processes that might be obscured by moderate-resolution data (Fassnacht et al., 2021).

One important limitation of this study is the lack of *in-situ* vegetation observations for evaluation. Chávez et al. (2022) previously addressed this issue, presenting PhenoCam images from the study region that show significant vegetation browning starting in December 2020, with a pronounced decline in vegetation greenness by January 2021. This is consistent with the patterns observed in our analysis. Furthermore, Fuentes et al. (2024a) analysed Landsat-based NDVI changes, reporting similar drought-driven vegetation declines during the same period. However, there remains an urgent need for enhanced ground-based monitoring in the region. While a PhenoCam network is currently under development in Chile (Chávez et al., 2020), their records start in 2023. Additionally, flux towers have been installed, but most are concentrated in southern Chile, leaving central Chile underrepresented in *in-situ* vegetation monitoring.

The observed differences in browning and recovery times between NDVI, LAI, and GPP may be caused by their distinct biophysical sensitivities. NDVI responds rapidly to changes in canopy chlorophyll

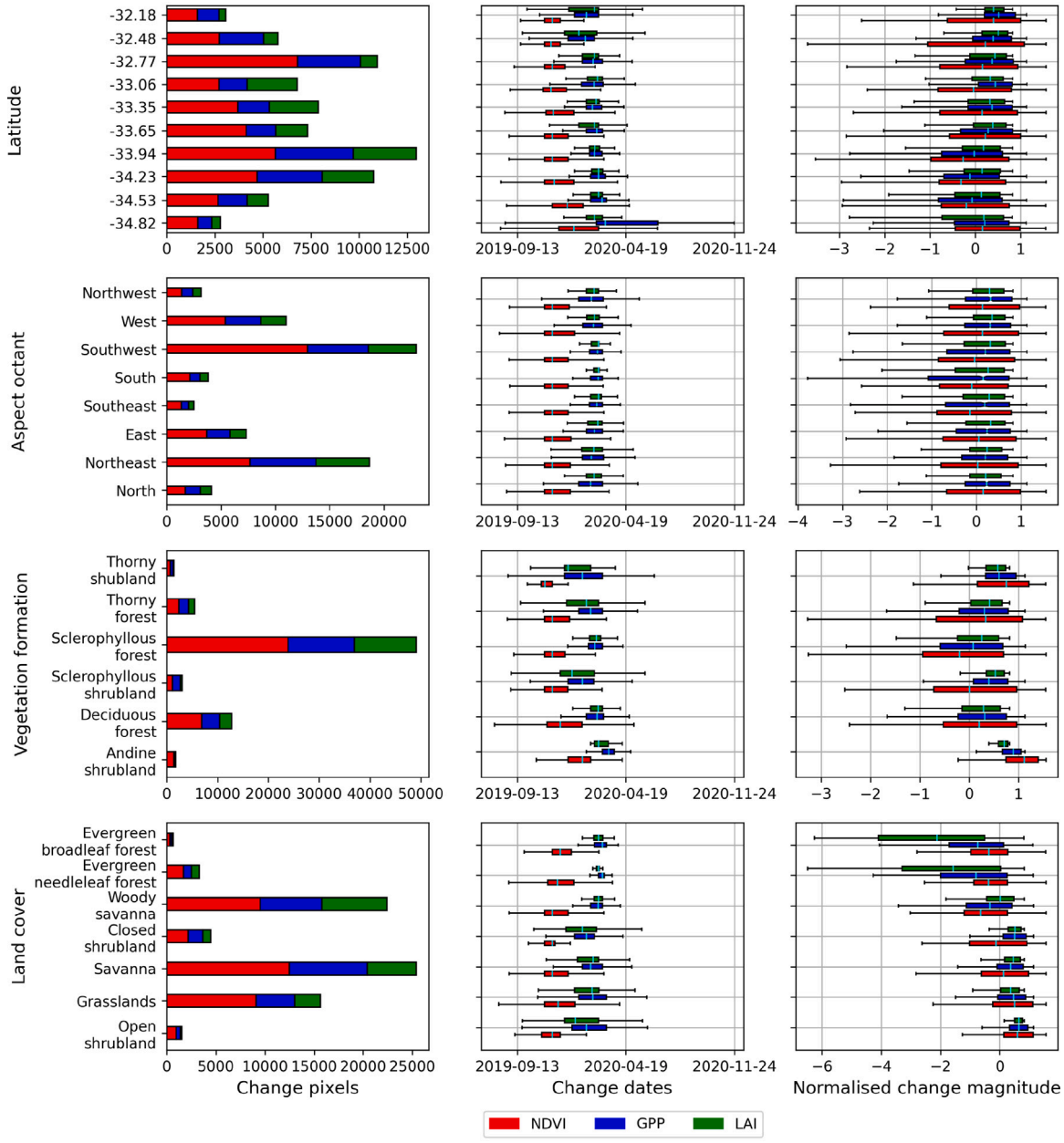

Fig. 13. Stacked bar plots of change pixels (left column panel) and boxplots of change dates (middle column panel) and normalised magnitudes of change (right column panel) for NDVI, GPP, and LAI across different latitudes (top panel), aspect octants (second row panel), vegetation formations (third row panel), and land cover classes (bottom panel).

content, making it effective for detecting short-term fluctuations but prone to saturation in dense vegetation (Pettorelli et al., 2005). LAI, which reflects total leaf area, captures structural vegetation changes and typically recovers more slowly than NDVI, as leaf development lags behind initial greening (Myneni et al., 2002). GPP, representing vegetation carbon assimilation, integrates both structural and physiological factors, providing insight into functional recovery beyond greenness alone (Running et al., 2000; Anav et al., 2015). These differences highlight the complementary roles of NDVI, LAI, and GPP in assessing vegetation changes, with NDVI capturing early responses, LAI reflecting structural changes, and GPP indicating productivity shifts. This study empirically evidences a sequence in vegetation's response to disturbances: vegetation vigour is initially impacted by severe dry conditions, with structural changes becoming evident some months later. However, not all changes in vegetation vigour propagate to structural or functional shifts. Approximately 60% of the area showing changes in vegetation vigour (NDVI) also exhibited changes in GPP, while 44% showed changes in LAI. These shifts in productivity and structural indicators occurred with an average delay of about 2.1 months later.

However, LAI and GPP estimates are subject to inherent uncertainties that must be considered. LAI, often derived from radiative transfer models, is influenced by model assumptions, sensor limitations, and biome-specific parameterisations (Myneni and Park, 2015). Despite these challenges, studies have reported reasonably good agreement between LAI estimates and field observations across different land cover types (Garrigues et al., 2008; Hill et al., 2006). Similarly, GPP estimates are affected by uncertainties related to input data quality, model parameterisation, and validation constraints. For instance, Zhang and Ye (2022) found that machine learning-based GPP estimates exhibited an average uncertainty of 14.3%, with variations across biomes. These uncertainties underscore the need for careful interpretation of LAI and GPP results. Nevertheless, these remotely sensed products remain

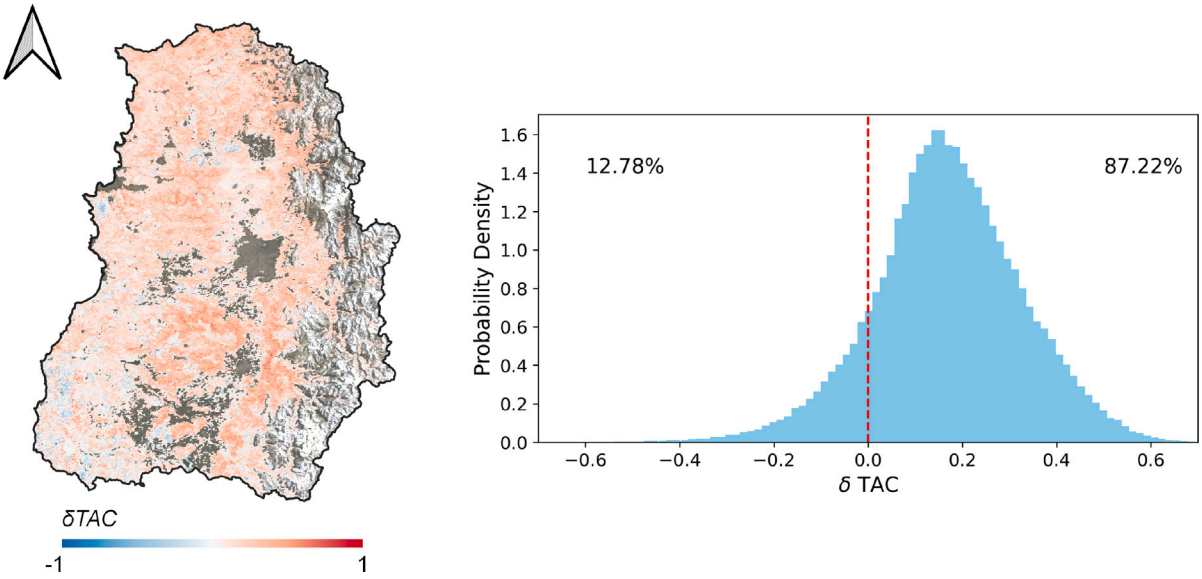

Fig. 14. Spatial distribution of δTAC for kNDVI between the periods 2000–2012 and 2013–2024 (left), and probability density distribution for the study region (right). Values in the right panel indicate the percentage of pixels with positive and negative δTAC values.

invaluable for large-scale ecosystem monitoring, providing critical insights into vegetation dynamics, carbon fluxes, and climate change impacts.

4.2. Factors conditioning vegetation vulnerability

Among the applications that arise from assessing drought propagation is the potential to study factors that may either attenuate or exacerbate drought impacts on the systems under study. In this case, vegetation vulnerability may be influenced by multiple factors, such as latitudes, topography, vegetation type, and land cover (Navas et al., 2008; Gonzalez et al., 2010; von Keyserlingk et al., 2021; Wei et al., 2022). However, further investigation into additional factors, such as soil properties and specific vegetation traits, which may exhibit higher spatial variability, could provide deeper insight into vegetation responses to drought. This will be addressed in future works using higher-resolution products.

Understanding the factors that shape drought propagation can guide resource prioritisation to bolster resilience against drought conditions and support the development of practices to enhance vegetation resilience (North et al., 2019; von Keyserlingk et al., 2021). For instance, in reforestation efforts, vegetation types adapted to dry conditions could be strategically selected for areas prone to droughts (Ramón Vallejo et al., 2012). Zheng et al. (2024), in their evaluation of drought responses in Argentina, identify shrublands as exhibiting the greatest resistance, consistent with the findings of the present study, while humid regions demonstrated the least drought tolerance. Additionally, understanding the lag in vegetation response and identifying vegetation types and locations where browning occurs sooner may enable preemptive responses in areas affected later, serving as an early warning system to improve drought management (Fuentes et al., 2022). For instance, faster vegetation responses to drought often occur northwards or in thorny and open shrublands, where their early affectation could trigger pre-emptive measures in systems with delayed drought responses, such as deciduous forests, Andean shrublands, and ecosystems in southern latitudes.

4.3. Vegetation resilience

Change detection algorithms coupled with temporal autocorrelation analysis can enhance vegetation resilience knowledge, serving as proxies for its study. By revealing delayed and incomplete recovery dynamics, as well as spatial patterns of resilience loss, these methods provide critical insights into ecosystem vulnerability. The limited area exhibiting both vegetation browning and subsequent recovery, combined with the observed lagged recovery of about four years post-disturbance and the shift of TAC towards higher values, raises concerns regarding vegetation resilience loss. Although similar trends have been documented in other ecosystems (Forzieri et al., 2022), the shift observed in the Mediterranean-climate region of central Chile is particularly acute, highlighting the effects of prolonged dry conditions that have persisted for over a decade (Garreaud et al., 2020). This region holds special significance as a biodiversity hotspot (Marchese, 2015) with many of its ecosystems, which host the analysed vegetation, classified as threatened under the International Union for Conservation of Nature (IUCN) criteria (Alaniz et al., 2016). Thus, any shifts or declines in vegetation health could impact both biodiversity and ecosystem services (Smith-Ramirez et al., 2023), underscoring the need for increased attention and action.

Although the prolonged dry conditions of the megadrought, which began in 2010, may have increased vegetation susceptibility, time series analysis does not show an abrupt decline in vegetation before 2019. The drought events of 2019 - 2020, however, triggered a rapid and widespread browning in vegetation. The exact causes behind this vegetation shift remain unclear. Allen et al. (2015) identifies several global vulnerability drivers of vegetation shift under climate warming, which may be relevant to study in this region.

While many studies indicate that vegetation “greening” remains the dominant global trend (Zhu et al., 2016; Zhang et al., 2017; Piao et al., 2020), vegetation browning has been observed in various regions (Cortés et al., 2021) and can sometimes be concealed in long-term trends (Pan et al., 2018). Central Chile is among the regions where browning events have been documented, highlighting a shift in vegetation resilience. Therefore, studies on vegetation vulnerability are essential to address the impacts of climate change and promote resilience and adaptability to water deficits.

5. Conclusions

Drought propagation was assessed using the CCDC algorithm to evaluate a widespread browning event in central Chile. Vegetation changes were tracked through NDVI, GPP, and LAI indices from MODIS satellites, and the CCDC algorithm estimated the extent, magnitude and timing changes while isolating other known sources of vegetation

degradation. Factors influencing vegetation vulnerability to drought and shifts in vegetation resilience were also analysed. Although this study focused on a specific region, the methodology can be applied broadly for drought propagation assessment in other areas. An empirical sequence in vegetation response to meteorological drought was observed, with initial vigour losses later translating into productivity reduction. However, not all losses in vegetation vigour led to subsequent productivity declines. About 19% of the study area exhibited declines in vegetation vigour, 12% in GPP, and 8% in LAI. Vegetation vigour responded to water deficits in roughly 6.6 months, while productivity changes lagged by about 8.7 months. Vegetation recovery, however, took an average of 3.6 years following the initial degradation, and the recovery extent was notably smaller than that of browning. Various factors such as topography, vegetation types, and latitude contributed to significant variations in the magnitude and timing of changes, highlighting key influences on vegetation vulnerability. A shift in vegetation resilience was also detected, underscoring the need for further studies to clarify the causes of browning and to develop strategies that promote vegetation resilience and adaptability in the face of climate change.

CRediT authorship contribution statement

Ignacio Fuentes: Writing – original draft, Visualization, Validation, Software, Methodology, Investigation, Funding acquisition, Formal analysis, Data curation, Conceptualization. **Javier Lopatin:** Writing – review & editing, Validation, Investigation, Data curation. **Mauricio Galleguillos:** Writing – review & editing, Supervision, Resources, Data curation. **James McPhee:** Writing – review & editing, Supervision, Resources, Funding acquisition, Data curation.

Code availability

The code associated with this project will be made available in the following repository: https://github.com/IFuentesSR/browning_assess

Declaration of competing interest

The authors declare the following financial interests/personal relationships which may be considered as potential competing interests: Ignacio Fuentes reports financial support was provided by National Commission for Scientific and Technological Research National Fund for Scientific and Technological Development. If there are other authors, they declare that they have no known competing financial interests or personal relationships that could have appeared to influence the work reported in this paper.

Acknowledgements

The researcher is supported by the ANID FONDECYT Postdoctoral Project N°3220317. Additionally, the reference dataset was supported by the 'SAMSARA' FONDEF IdeA I+D ID21I10102 project, ANID, Chile.

Appendix A. Supplementary data

Supplementary material related to this article can be found online at https://doi.org/10.1016/j.srs.2025.100219.

Data availability

Data used is publicly available and sources are properly cited.

References

Al-Nasrawi, A.K., Fuentes, I., Al-Shammari, D., 2021. Changes in mesopotamian wetlands: investigations using diverse remote sensing datasets. Wetlands 41 (7), 94.

Alaniz, A.J., Galleguillos, M., Perez-Quezada, J.F., 2016. Assessment of quality of input data used to classify ecosystems according to the IUCN red list methodology: The case of the central Chile hotspot. Biol. Cons. 204, 378–385.

Allen, C.D., Breshears, D.D., McDowell, N.G., 2015. On underestimation of global vulnerability to tree mortality and forest die-off from hotter drought in the Anthropocene. Ecosphere 6 (8), 1–55.

Anav, A., Friedlingstein, P., Beer, C., Ciais, P., Harper, A., Jones, C., Murray-Tortarolo, G., Papale, D., Parazoo, N.C., Peylin, P., et al., 2015. Spatiotemporal patterns of terrestrial gross primary production: A review. Rev. Geophys. 53 (3), 785–818.

Bannari, A., Morin, D., Bonn, F., Huete, A., 1995. A review of vegetation indices. Remote Sens. Rev. 13 (1–2), 95–120.

Beck, H.E., Zimmermann, N.E., McVicar, T.R., Vergopolan, N., Berg, A., Wood, E.F., 2018. Present and future Köppen-Geiger climate classification maps at 1-km resolution. Sci. Data 5 (1), 1–12.

Bowman, D.M., Moreira-Muñoz, A., Kolden, C.A., Chávez, R.O., Muñoz, A.A., Salinas, F., González-Reyes, Á., Rocco, R., de la Barrera, F., Williamson, G.J., et al., 2019. Human–environmental drivers and impacts of the globally extreme 2017 Chilean fires. Ambio 48 (4), 350–362.

Bullock, E.L., Healey, S.P., Yang, Z., Houborg, R., Gorelick, N., Tang, X., Andrianirina, C., 2022. Timeliness in forest change monitoring: A new assessment framework demonstrated using sentinel-1 and a continuous change detection algorithm. Remote Sens. Environ. 276, 113043.

Carrión, J.S., Fernández, S., Jiménez-Moreno, G., Fauquette, S., Gil-Romera, G., González-Sampériz, P., Finlayson, C., 2010. The historical origins of aridity and vegetation degradation in southeastern Spain. J. Arid. Environ. 74 (7), 731–736.

Chapungu, L., Nhamo, L., Gatti, R.C., 2020. Estimating biomass of savanna grasslands as a proxy of carbon stock using multispectral remote sensing. Remote. Sens. Applications: Soc. Environ. 17, 100275.

Chávez, R.O., Estay, S.A., Lastra, J.A., Riquelme, C.G., Olea, M., Aguayo, J., Decuyper, M., 2022. npphen: an R-package for detecting and mapping extreme vegetation anomalies based on remotely sensed phenological variability. Remote. Sens. 15 (1), 73.

Chávez, R.O., Olea, M., Lastra, J., Bruna, S., Valencia, D., 2020. Towards an integrated land-surface-phenology monitoring system for Chile: advances on remote sensing based platforms and phenocam field network. In: GEO BON Open Science Conference and All Hands Meeting 2020. GEO BON.

Chelli-Chaabouni, A., 2013. Mechanisms and adaptation of plants to environmental stress: a case of woody species. In: Physiological Mechanisms and Adaptation Strategies in Plants under Changing Environment: Volume 1. Springer, pp. 1–24.

Chen, S., Huang, Y., Wang, G., 2021. Detecting drought-induced GPP spatiotemporal variabilities with sun-induced chlorophyll fluorescence during the 2009/2010 droughts in China. Ecol. Indic. 121, 107092.

Cortés, J., Mahecha, M.D., Reichstein, M., Myneni, R.B., Chen, C., Brenning, A., 2021. Where are global vegetation greening and browning trends significant? Geophys. Res. Lett. 48 (6), e2020GL091496.

De Jong, R., Verbesselt, J., Schaepman, M.E., De Bruin, S., 2012. Trend changes in global greening and browning: contribution of short-term trends to longer-term change. Global Change Biol. 18 (2), 642–655.

Didan, K., Munoz, A.B., Solano, R., Huete, A., et al., 2015. MODIS vegetation index user's guide (MOD13 series). Univ. Arizona: Veg. Index Phenol. Lab 35, 2–33.

Duffie, J.A., Beckman, W.A., Blair, N., 2020. Solar Engineering of Thermal Processes, Photovoltaics and Wind. John Wiley & Sons.

Fang, X., Zhu, Q., Ren, L., Chen, H., Wang, K., Peng, C., 2018. Large-scale detection of vegetation dynamics and their potential drivers using MODIS images and BFAST: A case study in Quebec, Canada. Remote Sens. Environ. 206, 391–402.

Fassnacht, F.E., Schmidt-Riese, E., Kattenborn, T., Hernández, J., 2021. Explaining sentinel 2-based dNBR and RdNBR variability with reference data from the bird's eye (UAS) perspective. Int. J. Appl. Earth Obs. Geoinf. 95, 102262.

Forzieri, G., Dakos, V., McDowell, N.G., Ramdane, A., Cescatti, A., 2022. Emerging signals of declining forest resilience under climate change. Nature 608 (7923), 534–539.

Frampton, W.J., Dash, J., Watmough, G., Milton, E.J., 2013. Evaluating the capabilities of sentinel-2 for quantitative estimation of biophysical variables in vegetation. ISPRS J. Photogramm. Remote Sens. 82, 83–92.

Francini, S., McRoberts, R.E., Giannetti, F., Mencucci, M., Marchetti, M., Scarascia Mugnozza, G., Chirici, G., 2020. Near-real time forest change detection using PlanetScope imagery. Eur. J. Remote. Sens. 53 (1), 233–244.

Friedl, M., Sulla-Menashe, D., 2019. MCD12Q1 MODIS/Terra+ aqua land cover type yearly L3 global 500 m SIN grid V006. NASA EOSDIS Land Process. DAAC 10, 200.

Frolking, S., Palace, M.W., Clark, D., Chambers, J.Q., Shugart, H., Hurtt, G.C., 2009. Forest disturbance and recovery: A general review in the context of spaceborne remote sensing of impacts on aboveground biomass and canopy structure. J. Geophys. Research: Biogeosciences 114 (G2).

Fuentes, I., Lopatin, J., Galleguillos, M., Ceballos-Comisso, A., Eyheramendy, S., Carrasco, R., 2024a. Is the change deforestation? Using time-series analysis of satellite data to disentangle deforestation from other forest degradation causes. Remote. Sens. Applications: Soc. Environ. 35, 101210.

Fuentes, I., Padarian, J., Vervoort, R.W., 2022. Spatial and temporal global patterns of drought propagation. Front. Environ. Sci. 10, http://dx.doi.org/10.3389/fenvs.2022.788248, URL https://www.frontiersin.org/article/10.3389/fenvs.2022.788248.

Fuentes, I., Vervoort, R.W., McPhee, J., 2024b. Global evapotranspiration models and their performance at different spatial scales: Contrasting a latitudinal gradient against global catchments. J. Hydrol. 628, 130477.

Garreaud, R.D., Boisier, J.P., Rondanelli, R., Montecinos, A., Sepúlveda, H.H., Veloso-Aguila, D., 2020. The central Chile mega drought (2010–2018): a climate dynamics perspective. Int. J. Climatol. 40 (1), 421–439.

Garrigues, S., Shabanov, N., Swanson, K., Morisette, J., Baret, F., Myneni, R., 2008. Intercomparison and sensitivity analysis of leaf area index retrievals from LAI-2000, AccuPAR, and digital hemispherical photography over croplands. Agricult. Forest. Meterol. 148 (8–9), 1193–1209.

Glantz, S.A., et al., 2002. Primer of Biostatistics. McGraw-Hill.

Gonzalez, P., Neilson, R.P., Lenihan, J.M., Drapek, R.J., 2010. Global patterns in the vulnerability of ecosystems to vegetation shifts due to climate change. Glob. Ecol. Biogeogr. 19 (6), 755–768.

Gorelick, N., Hancher, M., Dixon, M., Ilyushchenko, S., Thau, D., Moore, R., 2017. Google earth engine: Planetary-scale geospatial analysis for everyone. Remote Sens. Environ. 202, 18–27.

Guenang, G.M., Kamga, F.M., 2014. Computation of the standardized precipitation index (SPI) and its use to assess drought occurrences in Cameroon over recent decades. J. Appl. Meteorol. Clim. 53 (10), 2310–2324.

Hammer, D., Kraft, R., Wheeler, D., 2014. Alerts of forest disturbance from MODIS imagery. Int. J. Appl. Earth Obs. Geoinf. 33, 1–9.

Hijmans, R.J., Cameron, S.E., Parra, J.L., Jones, P.G., Jarvis, A., 2005. Very high resolution interpolated climate surfaces for global land areas. Int. J. Climatology: A J. R. Meteorol. Soc. 25 (15), 1965–1978.

Hill, M.J., Senarath, U., Lee, A., Zeppel, M., Nightingale, J.M., Williams, R.D.J., McVicar, T.R., 2006. Assessment of the MODIS LAI product for Australian ecosystems. Remote Sens. Environ. 101 (4), 495–518.

Hollunder, R.K., Mariotte, P., Carrijo, T.T., Holmgren, M., Luber, J., Stein-Soares, B., Guidoni-Martins, K.G., Ferreira-Santos, K., Scarano, F.R., Garbin, M.L., 2021. Topography and vegetation structure mediate drought impacts on the understory of the South American Atlantic forest. Sci. Total Environ. 766, 144234.

Homolová, L., Malenovskỳ, Z., Clevers, J.G., García-Santos, G., Schaepman, M.E., 2013. Review of optical-based remote sensing for plant trait mapping. Ecol. Complex. 15, 1–16.

Jiang, W., Wang, L., Zhang, M., Yao, R., Chen, X., Gui, X., Sun, J., Cao, Q., 2021. Analysis of drought events and their impacts on vegetation productivity based on the integrated surface drought index in the Hanjiang River Basin, China. Atmos. Res. 254, 105536.

Kofinas, G.P., 2009. Adaptive co-management in social-ecological governance. In: Principles of Ecosystem Stewardship. Springer, pp. 77–101.

Konings, A.G., Saatchi, S.S., Frankenberg, C., Keller, M., Leshyk, V., Anderegg, W.R., Humphrey, V., Matheny, A.M., Trugman, A., Sack, L., et al., 2021. Detecting forest response to droughts with global observations of vegetation water content. Global Change Biol. 27 (23), 6005–6024.

Kumar, R., Kumar, A., Saikia, P., 2022. Deforestation and forests degradation impacts on the environment. In: Environmental Degradation: Challenges and Strategies for Mitigation. Springer, pp. 19–46.

Lambert, J., Drenou, C., Denux, J.-P., Balent, G., Cheret, V., 2013. Monitoring forest decline through remote sensing time series analysis. GIScience & Remote. Sens. 50 (4), 437–457.

Letts, M.G., Johnson, D.R., Coburn, C.A., 2010. Drought stress ecophysiology of shrub and grass functional groups on opposing slope aspects of a temperate grassland valley. Botany 88 (9), 850–866.

Li, L., She, D., Zheng, H., Lin, P., Yang, Z.-L., 2020. Elucidating diverse drought characteristics from two meteorological drought indices (SPI and SPEI) in China. J. Hydrometeorol. 21 (7), 1513–1530.

Lian, T., Wang, J., Chen, D., Liu, T., Wang, D., 2023. A strong 2023/24 El Niño is staged by tropical Pacific ocean heat content buildup. Ocean- Land- Atmosphere Res. 2, 0011.

Liu, Q.-q., Chen, L., Li, J.-c., 2001. Influences of slope gradient on soil erosion. Appl. Math. Mech. 22, 510–519.

Liu, Y., Li, Z., Chen, Y., 2021. Continuous warming shift greening towards browning in the Southeast and Northwest High Mountain Asia. Sci. Rep. 11 (1), 17920.

Liu, Q., Peng, C., Schneider, R., Cyr, D., Liu, Z., Zhou, X., Du, M., Li, P., Jiang, Z., McDowell, N.G., et al., 2023a. Vegetation browning: global drivers, impacts, and feedbacks. Trends Plant Sci. 28 (9), 1014–1032.

Liu, X., Sun, G., Fu, Z., Ciais, P., Feng, X., Li, J., Fu, B., 2023b. Compound droughts slow down the greening of the earth. Global Change Biol. 29 (11), 3072–3084.

Liu, Y.Y., van Dijk, A.I., McCabe, M.F., Evans, J.P., de Jeu, R.A., 2013. Global vegetation biomass change (1988–2008) and attribution to environmental and human drivers. Glob. Ecol. Biogeogr. 22 (6), 692–705.

Liu, Y., Xie, M., Wang, H., Hu, R., Ji, Y., Liu, Q., 2024. Vegetation resilience assessment and its climatic driving factors: Evidence from surface coal mines in northern China. Sci. Total Environ. 173803.

Lizundia-Loiola, J., Otón, G., Ramo, R., Chuvieco, E., 2020. A spatio-temporal active-fire clustering approach for global burned area mapping at 250 m from MODIS data. Remote Sens. Environ. 236, 111493.

Luebert, F., Pliscoff, P., 2022. The vegetation of Chile and the EcoVeg approach in the context of the international vegetation classification project. Veg. Classif. Surv. 3, 15–28.

Marchese, C., 2015. Biodiversity hotspots: A shortcut for a more complicated concept. Glob. Ecol. Conserv. 3, 297–309.

McKee, T.B., Doesken, N.J., Kleist, J., et al., 1993. The relationship of drought frequency and duration to time scales. In: Proceedings of the 8th Conference on Applied Climatology, Vol. 17, No. 22. Boston, pp. 179–183.

Miranda, A., Lara, A., Altamirano, A., Di Bella, C., González, M.E., Camarero, J.J., 2020. Forest browning trends in response to drought in a highly threatened mediterranean landscape of South America. Ecol. Indic. 115, 106401.

Miranda, A., Syphard, A.D., Berdugo, M., Carrasco, J., Gómez-González, S., Ovalle, J.F., Delpiano, C.A., Vargas, S., Squeo, F.A., Miranda, M.D., et al., 2023. Widespread synchronous decline of Mediterranean-type forest driven by accelerated aridity. Nat. Plants 9 (11), 1810–1817.

Morton, D.C., DeFries, R.S., Shimabukuro, Y.E., Anderson, L.O., Del Bon Espírito-Santo, F., Hansen, M., Carroll, M., 2005. Rapid assessment of annual deforestation in the Brazilian Amazon using MODIS data. Earth Interactions 9 (8), 1–22.

Murthy, K., Bagchi, S., 2018. Spatial patterns of long-term vegetation greening and browning are consistent across multiple scales: Implications for monitoring land degradation. Land Degrad. Dev. 29 (8), 2485–2495.

Myers, N., Mittermeier, R.A., Mittermeier, C.G., Da Fonseca, G.A., Kent, J., 2000. Biodiversity hotspots for conservation priorities. Nature 403 (6772), 853–858.

Myneni, R.B., Hoffman, S., Knyazikhin, Y., Privette, J., Glassy, J., Tian, Y., Wang, Y., Song, X., Zhang, Y., Smith, G., et al., 2002. Global products of vegetation leaf area and fraction absorbed PAR from year one of MODIS data. Remote Sens. Environ. 83 (1–2), 214–231.

Myneni, R., Park, Y., 2015. MODIS collection 6 (C6) LAI/FPAR product user's guide.

Navas, A., Machín, J., Beguería, S., López-Vicente, M., Gaspar, L., 2008. Soil properties and physiographic factors controlling the natural vegetation re-growth in a disturbed catchment of the Central Spanish Pyrenees. Agrofor. Syst. 72, 173–185.

North, M.P., Stevens, J.T., Greene, D.F., Coppoletta, M., Knapp, E.E., Latimer, A.M., Restaino, C.M., Tompkins, R.E., Welch, K.R., York, R.A., et al., 2019. Tamm review: Reforestation for resilience in dry western US forests. Forest Ecol. Manag. 432, 209–224.

Olofsson, P., Foody, G.M., Herold, M., Stehman, S.V., Woodcock, C.E., Wulder, M.A., 2014. Good practices for estimating area and assessing accuracy of land change. Remote Sens. Environ. 148, 42–57.

Pan, N., Feng, X., Fu, B., Wang, S., Ji, F., Pan, S., 2018. Increasing global vegetation browning hidden in overall vegetation greening: Insights from time-varying trends. Remote Sens. Environ. 214, 59–72.

Pausas, J.G., Keeley, J.E., 2021. Wildfires and global change. Front. Ecol. Environ. 19 (7), 387–395.

Peters, A.J., Walter-Shea, E.A., Ji, L., Vina, A., Hayes, M., Svoboda, M.D., 2002. Drought monitoring with NDVI-based standardized vegetation index. Photogramm. Eng. Remote Sens. 68 (1), 71–75.

Pettorelli, N., Vik, J.O., Mysterud, A., Gaillard, J.-M., Tucker, C.J., Stenseth, N.C., 2005. Using the satellite-derived NDVI to assess ecological responses to environmental change. Trends Ecol. Evolut. 20 (9), 503–510.

Piao, S., Wang, X., Park, T., Chen, C., Lian, X., He, Y., Bjerke, J.W., Chen, A., Ciais, P., Tømmervik, H., et al., 2020. Characteristics, drivers and feedbacks of global greening. Nat. Rev. Earth & Environ. 1 (1), 14–27.

Ramón Vallejo, V., Smanis, A., Chirino, E., Fuentes, D., Valdecantos, A., Vilagrosa, A., 2012. Perspectives in dryland restoration: approaches for climate change adaptation. New For. 43 (5), 561–579.

Running, S.W., Thornton, P.E., Nemani, R., Glassy, J.M., 2000. Global terrestrial gross and net primary productivity from the earth observing system. In: Methods in Ecosystem Science. Springer, pp. 44–57.

Schultz, M., Clevers, J.G., Carter, S., Verbesselt, J., Avitabile, V., Quang, H.V., Herold, M., 2016. Performance of vegetation indices from Landsat time series in deforestation monitoring. Int. J. Appl. Earth Obs. Geoinf. 52, 318–327.

Seleiman, M.F., Al-Suhaibani, N., Ali, N., Akmal, M., Alotaibi, M., Refay, Y., Dindaroglu, T., Abdul-Wajid, H.H., Battaglia, M.L., 2021. Drought stress impacts on plants and different approaches to alleviate its adverse effects. Plants 10 (2), 259.

Smith, A.M., Kolden, C.A., Tinkham, W.T., Talhelm, A.F., Marshall, J.D., Hudak, A.T., Boschetti, L., Falkowski, M.J., Greenberg, J.A., Anderson, J.W., et al., 2014. Remote sensing the vulnerability of vegetation in natural terrestrial ecosystems. Remote Sens. Environ. 154, 322–337.

Smith-Ramirez, C., Grez, A., Galleguillos, M., Cerda, C., Ocampo-Melgar, A., Miranda, M.D., Munoz, A.A., Rendon-Funes, A., Diaz, I., Cifuentes, C., et al., 2023. Ecosystem services of Chilean sclerophyllous forests and shrublands on the verge of collapse: A review. J. Arid. Environ. 211, 104927.

Takahashi, F., Kuromori, T., Urano, K., Yamaguchi-Shinozaki, K., Shinozaki, K., 2020. Drought stress responses and resistance in plants: From cellular responses to long-distance intercellular communication. Front. Plant Sci. 11, 556972.

Thornton, P.K., Ericksen, P.J., Herrero, M., Challinor, A.J., 2014. Climate variability and vulnerability to climate change: a review. Global Change Biol. 20 (11), 3313–3328.
Van Loon, A.F., Kchouk, S., Matanó, A., Tootoonchi, F., Garreton, C.A., Hassaballah, K.E., Wu, M., Wens, M.L., Shyrokaya, A., Ridolfi, E., et al., 2024. Drought as a continuum: memory effects in interlinked hydrological, ecological, and social systems. Nat. Hazards Earth Syst. Sci. 24 (9), 3173–3205.
Vicca, S., Balzarolo, M., Filella, I., Granier, A., Herbst, M., Knohl, A., Longdoz, B., Mund, M., Nagy, Z., Pintér, K., et al., 2016. Remotely-sensed detection of effects of extreme droughts on gross primary production. Sci. Rep. 6 (1), 28269.
Vicente-Serrano, S.M., Cabello, D., Tomás-Burguera, M., Martín-Hernández, N., Beguería, S., Azorin-Molina, C., El Kenawy, A., 2015. Drought variability and land degradation in semiarid regions: Assessment using remote sensing data and drought indices (1982–2011). Remote. Sens. 7 (4), 4391–4423.
Vicente-Serrano, S.M., Gouveia, C., Camarero, J.J., Beguería, S., Trigo, R., López-Moreno, J.I., Azorín-Molina, C., Pasho, E., Lorenzo-Lacruz, J., Revuelto, J., et al., 2013. Response of vegetation to drought time-scales across global land biomes. Proc. Natl. Acad. Sci. 110 (1), 52–57.
Vicente-Serrano, S.M., Quiring, S.M., Peña-Gallardo, M., Yuan, S., Domínguez-Castro, F., 2020. A review of environmental droughts: Increased risk under global warming? Earth-Sci. Rev. 201, 102953.
Vilanova, R.S., Delgado, R.C., de Andrade, C.F., dos Santos, G.L., Magistrali, I.C., de Oliveira, C.M.M., Teodoro, P.E., Silva, G.F.C., da Silva Junior, C.A., de Ávila Rodrigues, R., 2021. Vegetation degradation in ENSO events: Drought assessment, soil use and vegetation evapotranspiration in the Western Brazilian Amazon. Remote. Sens. Applications: Soc. Environ. 23, 100531.
von Keyserlingk, J., De Hoop, M., Mayor, A., Dekker, S., Rietkerk, M., Foerster, S., 2021. Resilience of vegetation to drought: Studying the effect of grazing in a Mediterranean rangeland using satellite time series. Remote Sens. Environ. 255, 112270.
Wang, W., Ertsen, M.W., Svoboda, M.D., Hafeez, M., 2016. Propagation of drought: from meteorological drought to agricultural and hydrological drought. Hindawi 2016.
Wanyama, D., Moore, N.J., Dahlin, K.M., 2020. Persistent vegetation greening and browning trends related to natural and human activities in the mount Elgon ecosystem. Remote. Sens. 12 (13), 2113.
Watch, G.F., 2002. Global Forest Watch. World Resources Institute, Washington, DC, Available from http://www.global-forestwatch.org. (accessed March 2002).
Wei, X., Huang, S., Huang, Q., Liu, D., Leng, G., Yang, H., Duan, W., Li, J., Bai, Q., Peng, J., 2022. Analysis of vegetation vulnerability dynamics and driving forces to multiple drought stresses in a changing environment. Remote. Sens. 14 (17), 4231.
Weinans, E., Quax, R., van Nes, E.H., Leemput, I.A.v.d., 2021. Evaluating the performance of multivariate indicators of resilience loss. Sci. Rep. 11 (1), 9148.
Xie, Y., Sha, Z., Yu, M., 2008. Remote sensing imagery in vegetation mapping: a review. J. Plant Ecol. 1 (1), 9–23.
Yamazaki, D., Ikeshima, D., Tawatari, R., Yamaguchi, T., O'Loughlin, F., Neal, J.C., Sampson, C.C., Kanae, S., Bates, P.D., 2017. A high-accuracy map of global terrain elevations. Geophys. Res. Lett. 44 (11), 5844–5853.
Yang, J., Weisberg, P.J., Bristow, N.A., 2012. Landsat remote sensing approaches for monitoring long-term tree cover dynamics in semi-arid woodlands: Comparison of vegetation indices and spectral mixture analysis. Remote Sens. Environ. 119, 62–71.
Yin, J., Bauerle, T.L., 2017. A global analysis of plant recovery performance from water stress. Oikos 126 (10), 1377–1388.
Zargar, A., Sadiq, R., Naser, B., Khan, F.I., 2011. A review of drought indices. Environ. Rev. 19 (NA), 333–349.
Zeng, Y., Hao, D., Huete, A., Dechant, B., Berry, J., Chen, J.M., Joiner, J., Frankenberg, C., Bond-Lamberty, B., Ryu, Y., et al., 2022. Optical vegetation indices for monitoring terrestrial ecosystems globally. Nat. Rev. Earth & Environ. 3 (7), 477–493.
Zhang, X., Friedl, M.A., Schaaf, C.B., Strahler, A.H., Hodges, J.C., Gao, F., Reed, B.C., Huete, A., 2003. Monitoring vegetation phenology using MODIS. Remote Sens. Environ. 84 (3), 471–475.
Zhang, X., Hao, Z., Singh, V.P., Zhang, Y., Feng, S., Xu, Y., Hao, F., 2022. Drought propagation under global warming: Characteristics, approaches, processes, and controlling factors. Sci. Total Environ. 838, 156021.
Zhang, Y., Kong, D., Gan, R., Chiew, F.H., McVicar, T.R., Zhang, Q., Yang, Y., 2019. Coupled estimation of 500 m and 8-day resolution global evapotranspiration and gross primary production in 2002–2017. Remote Sens. Environ. 222, 165–182.
Zhang, Y., Song, C., Band, L.E., Sun, G., Li, J., 2017. Reanalysis of global terrestrial vegetation trends from MODIS products: Browning or greening? Remote Sens. Environ. 191, 145–155.
Zhang, Y., Ye, A., 2022. Uncertainty analysis of multiple terrestrial gross primary productivity products. Glob. Ecol. Biogeogr. 31 (11), 2204–2218.
Zheng, W., Askari, K., Song, C., Shi, P., Ge, W., Shi, S., Chu, J., Chen, H., Wang, F., 2024. Increasing vulnerability of vegetation to Meteorological and Groundwater drought: A Case study in Argentina. J. Hydrology: Reg. Stud. 55, 101931.
Zhu, Z., 2017. Change detection using landsat time series: A review of frequencies, preprocessing, algorithms, and applications. ISPRS J. Photogramm. Remote Sens. 130, 370–384.
Zhu, Z., Piao, S., Myneni, R.B., Huang, M., Zeng, Z., Canadell, J.G., Ciais, P., Sitch, S., Friedlingstein, P., Arneth, A., et al., 2016. Greening of the Earth and its drivers. Nat. Clim. Chang. 6 (8), 791–795.
Zhu, Z., Woodcock, C.E., 2014. Continuous change detection and classification of land cover using all available Landsat data. Remote Sens. Environ. 144, 152–171.
Zhu, Z., Zhang, J., Yang, Z., Aljaddani, A.H., Cohen, W.B., Qiu, S., Zhou, C., 2020. Continuous monitoring of land disturbance based on Landsat time series. Remote Sens. Environ. 238, 111116.